



AMERICAN UNIVERSITY OF BEIRUT

MECHANICAL MODELING OF STEEL TOP AND SEAT  
ANGLE CONNECTIONS SUBJECTED TO FIRE LOADING

by  
SANA NAJIB EL KALASH

A thesis  
submitted in partial fulfillment of the requirements  
for the degree of Master of Engineering  
to the Department of Civil and Environmental Engineering  
of the Faculty of Engineering and Architecture  
at the American University of Beirut

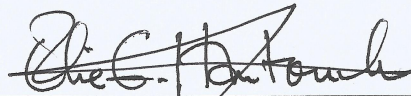
Beirut, Lebanon  
February 2016

AMERICAN UNIVERSITY OF BEIRUT

MECHANICAL MODELING OF STEEL TOP AND SEAT  
ANGLE CONNECTIONS SUBJECTED TO FIRE LOADING

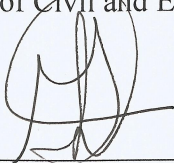
by  
SANA NAJIB EL KALASH

Approved by:



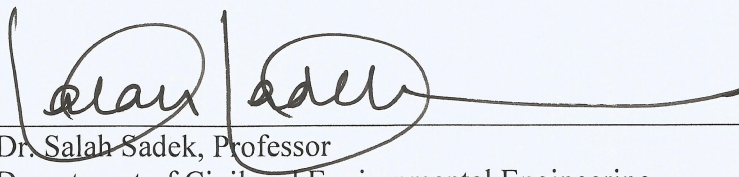
Dr. Elie Hantouche, Assistant Professor  
Department of Civil and Environmental Engineering

Advisor



Dr. Ghassan Chehab, Associate Professor  
Department of Civil and Environmental Engineering

Member of Committee



Dr. Salah Sadek, Professor  
Department of Civil and Environmental Engineering

Member of Committee

Date of thesis defense: 05 February 2016

# AMERICAN UNIVERSITY OF BEIRUT

## THESIS, DISSERTATION, PROJECT RELEASE FORM

Student Name: \_\_\_\_\_  
Last First Middle

Master's Thesis       Master's Project       Doctoral Dissertation

I authorize the American University of Beirut to: (a) reproduce hard or electronic copies of my thesis, dissertation, or project; (b) include such copies in the archives and digital repositories of the University; and (c) make freely available such copies to third parties for research or educational purposes.

I authorize the American University of Beirut, **three years after the date of submitting my thesis, dissertation, or project**, to: (a) reproduce hard or electronic copies of it; (b) include such copies in the archives and digital repositories of the University; and (c) make freely available such copies to third parties for research or educational purposes.

\_\_\_\_\_  
Signature

\_\_\_\_\_  
Date

This form is signed when submitting the thesis, dissertation, or project to the University Libraries

## ACKNOWLEDGMENTS

First and foremost, I would like to acknowledge and thank my advisor, Dr. Elie Hantouche. His expertise, dedication and enthusiasm were essential in the successful development of this research work. I appreciate his constant support and valuable critics which helped me develop my research skills, and knowledge throughout the time spent at the American University of Beirut.

My recognition and gratitude are addressed to my committee Dr. Ghassan Chehab and Dr. Salah Sadek.

Furthermore, I would like to gratefully acknowledge the financial support provided by the American University of Beirut Research Board under grant No.21113-102726, and by the Lebanese National Council for Scientific Research (LNCSR) under grant No. 103091-22968.

Finally, I would like to express gratitude to my family and friends for their support in the pursuit of my degree.

## AN ABSTRACT OF THE THESIS OF

Sana Najib El Kalash for Master of Engineering  
Major: Civil and Environmental Engineering

Title: Mechanical Modeling of Steel Top and Seat Angle Connections Subjected to Fire Loading

The finite element (FE) simulations and the experimental results are used to develop a mechanical model to predict the axial forces and rotations of top and seat angle connections with and without web angles subjected to elevated temperatures. The model incorporates the overall connection and column-beam rotation of key component elements, and includes nonlinear behavior of bolts and base materials at elevated temperatures and some major geometric parameters that impact the behavior of such connections when exposed to fire. This includes load ratio, beam length, angle thickness, and gap distance.

The mechanical model consists of multi-linear and nonlinear springs that predict each component stiffness, strength, and rotation. The beam stiffness is included in the proposed model to predict beam-column connection assembly rotation and thermal axial forces and their effect on the connection response. The proposed model is validated against experimental results available in the literature and FE simulations developed as a part of this study.

The proposed model provides important insights into fire-induced axial forces and rotations and their implications on the design of steel bolted top and seat angle connections with and without web angles.

# CONTENTS

ACKNOWLEDGMENTS .....	v
ABSTRACT .....	vi
ILLUSTRATIONS .....	ix
TABLES .....	xi
LIST OF ABBREVIATIONS .....	xii

## Chapter

INTRODUCTION .....	1
FE MODEL OF ISOLATED TOP AND SEAT ANGLE CONNECTION .....	4
A. Development of the FE model .....	4
1. Geometry of connection components.....	4
2. Geometric and force boundary conditions .....	6
3. Material Properties .....	6
4. Model discretization.....	7
5. Analysis procedure.....	7
B. Comparison of FE predictions with experiments .....	8
TOP AND SEAT ANGLE CONNECTION ASSEMBLY: EVALUATIONS OF DEMAND .....	11
A. Description of the connection assembly model .....	11
B. Effect of key parameters and connection details.....	14
1. Load ratio .....	14
2. Beam length .....	15

3. Top and Seat Angle thickness .....	17
4. Gap distance.....	18
<b>MECHANICAL MODEL.....</b>	<b>21</b>
<b>A. Component stiffness.....</b>	<b>22</b>
1.Column web .....	22
2. Column flange.....	22
3. Top angle vertical leg.....	23
4. Top angle horizontal leg.....	24
5. Tension bolts .....	24
6. Shear bolts.....	24
7. Web angles .....	24
<b>B. Equivalent connection stiffness.....</b>	<b>25</b>
<b>C. Connection rotation .....</b>	<b>26</b>
1. Connection failure modes .....	28
2. Model performance .....	29
<b>D. Beam-column connection thermal axial force .....</b>	<b>31</b>
1. Behavioral characteristics of top and seat angle connections .....	32
2. Effect of web angles.....	39
3. Proposed model performance.....	40
<b>E. Automated procedure .....</b>	<b>51</b>
<b>SUMMARY, CONCLUSIONS AND RECOMMENDATIONS.....</b>	<b>54</b>
<b>BIBLIOGRAPHY .....</b>	<b>56</b>



## ILLUSTRATIONS

Figure	Page
1. Connection details in FE model: (a) Top and seat angle with web angles, (b) Top and seat angle without web angles.....	5
2. FE vs. Experiment: Temperature vs. rotation of connection: (a) Exp.1, (b) Exp.1-w, (c) Exp., (d) Exp.2-w.....	9
3. Von Mises stress contours vs. experimental results: (a) Tension bolt failure (Exp.1 and Exp.1-w), (b) Top angle failure (Exp.2 and Exp.2-w).....	10
4. Layout of connection assemblies used in parametric study.....	13
5. (a) Axial force for varying load ratio, (b) Connection Rotation for varying load ratio, (c) Axial force comparison with and without web angles (case 1 vs. case 2)...	15
6. (a) Axial force for varying beam length, (b) Connection Rotation for varying beam length, (c) Axial force comparison with and without web angles (case 7 vs. case 8).	16
7. (a) Axial force for varying angle thickness, (b) Rotation for varying angle thickness, (c) Axial force comparison with and without web angles (case 13 vs. case 14).....	17
8. (a) Axial force for varying gap distance, (b) Rotation for varying gap distance, (c) Axial force comparison with and without web angles (case 15 vs. case 16).....	19
9. Mechanical model: Components stiffnesses.....	21
10. Mechanical model: (a) Connection, (b) Top and seat angle, web angle.....	22
11. Connection detailing.....	26
12. Equivalent rotational system.....	27
13. Proposed model vs. FE vs. Experiment: Temperature vs. rotation of connection: (a) Exp.1, (b) Exp.1-w, (c) Exp.2, (d) Exp.2-w.....	30
14. Equivalent linear system.....	32
15. Beam area.....	40
16. FE vs. proposed model for case 1: (a) Axial Force, (b) Connection rotation.....	41

17.	FE vs. proposed model for case 2: (a) Axial Force, (b) Connection rotation.....	41
18.	FE vs. proposed model for case 3: (a) Axial Force, (b) Connection rotation.....	42
19.	FE vs. proposed model for case 4: (a) Axial Force, (b) Connection rotation.....	42
20.	FE vs. proposed model for case 5: (a) Axial Force, (b) Connection rotation.....	43
21.	FE vs. proposed model for case 6: (a) Axial Force, (b) Connection rotation.....	43
22.	FE vs. proposed model for case 7: (a) Axial Force, (b) Connection rotation.....	44
23.	FE vs. proposed model for case 8: (a) Axial Force, (b) Connection rotation.....	44
24.	FE vs. proposed model for case 9: (a) Axial Force, (b) Connection rotation.....	45
25.	FE vs. proposed model for case 10: (a) Axial Force, (b) Connection rotation.....	45
26.	FE vs. proposed model for case 11: (a) Axial Force, (b) Connection rotation.....	46
27.	FE vs. proposed model for case 12: (a) Axial Force, (b) Connection rotation.....	46
28.	FE vs. proposed model for case 13: (a) Axial Force, (b) Connection rotation.....	47
29.	FE vs. proposed model for case 14: (a) Axial Force, (b) Connection rotation.....	47
30.	FE vs. proposed model for case 15: (a) Axial Force, (b) Connection rotation.....	48
31.	FE vs. proposed model for case 16: (a) Axial Force, (b) Connection rotation.....	48
32.	FE vs. proposed model for W18x46 beam: (a) Axial Force, (b) Connection rotation	50
33.	FE vs. proposed model for W21x68 beam: (a) Axial Force, (b) Connection rotation	50
34.	Flowchart of the incremental mechanical model: (a) rotation, (b) axial force.....	52

## TABLES

Table		Page
1.	Parametric study cases using FE modeling.....	14
2.	FE results comparison of top and seat angle connection with and without web angles.....	20
3.	Experiment vs. FE vs. proposed model results of top and seat angle connection.....	31
4.	FE vs. proposed model results of top and seat angle connection assembly.....	49

## LIST OF ABBREVIATIONS

$A_b$  : beam area contributing to thermal induced axial force

$A_{bolt}$  : shear bolt area

$A_{bw}$  : area of beam web

$A_{bwa}$  : beam area contributing to thermal induced axial force including web angle effect

$b_{eff-cw}$  : effective length of column web

$b_{eff-wa}$  : effective length of web angles

$b_f$  : beam flange width

$b_{ta}$  : width of top angle

$d_b$  : diameter of bolt

$d_c$  : depth of the column

$d_{cw}$  : effective depth of column web

$e$  : distance between the bolt centerline and the upper edge of the angle

$E_b$  : modulus of elasticity of beam

$E_T$  : tangent modulus of elasticity

$F_{ub}$  : ultimate strength of bolts

$F_y$  : beam flange yield stress

$F_{yc}$  : column yield stress

$g$  : gage distance

$g_a$  : gage distance between bolt holes in angle

$h_b$  : beam depth.

$h_i$  : distance from component under consideration to beam bottom flange

$I_a$  : moment of inertia of angle leg

$I_b$  : moment of inertia of beam

$I_{bolt}$  : moment of inertia of tension bolt

$K$  : equivalent spring stiffness

$K_{cf}$  : flexural stiffness of column flange

$K_{cw}$  : column web stiffness

$k_{des}$  : design fillet size of the column

$K_i$  : stiffness of every component

$K_{rot}$  : equivalent rotational stiffness

$K_{sb}$  : shear bolt stiffness

$K_{tah}$  : top angle horizontal leg stiffness

$K_{tav}$  : stiffness of top angle vertical leg

$K_{tb}$  : tension bolt stiffness

$K_{wa}$  : web angles stiffness

$L$  : beam length

$L_b$  : tension bolt shank length

$l_{eff-cf}$  : effective length of column flange

$m$  : clear distance between top angle fillet and bolt centerline

$M_{app}$  : constant applied moment on beam due to gravity load

$M_f$  : moment applied at face of column

$M_p$  : plastic moment capacity

$M_{pr}$  : maximum expected moment at plastic hinge in beam

$M_{p-angle}$  : top angle plastic moment capacity

$M_{(T)}$  : applied moment on connection in function of  $T$

$m_{wa}$  : clear distance between web angle fillet and bolt centerline

$M_y$  : yielding moment capacity

$n_{sb}$  : number of shear bolts

$n_{tb}$  : number of tension bolts

$P_{abb}$  : applied force on bottom shear bolts

$P_{abf}$  : applied force on bottom beam flange

$P_{abw}$  : applied force on beam web

$P_{acf}$  : applied force on column flange

$P_{acw}$  : applied force on column web

$P_{asb}$  : applied force on shear bolt

$P_{atb}$  : applied force on top shear bolts

$P_{atf}$  : applied force on top beam flange

$P_{bfy}$  : beam flange yielding capacity

$P_{bwy}$  : beam web yielding capacity

$P_{ca}$  : thermal compressive axial force in angle

$P_{cfy}$  : column flange yielding capacity

$P_{crb}$  : critical beam flange local buckling force

$P_{cwy}$  : column web yielding capacity

$P_i$  : total axial force

$P_{\max(\text{compression})}$  : maximum compressive axial force

$P_{sb}$  : shear bolts capacity

$P_{ta}$  : applied force on top angle

$P_{tb}$  : applied force on tension bolt

$q_i$  : ratio of plastic strain to elastic strain at each temperature increment

$SB$  : gap distance between column and beam

$S_h$  : location of plastic hinge

$T$  : temperature

$t_{bw}$  : thickness of beam web

$t_{cf}$  : thickness of column flange

$t_{cw}$  : thickness of column web

$t_f$  : beam flange thickness

$t_{ta}$  : thickness of top angle

$t_{wa}$  : thickness of web angle

$V_h$  : shear force at plastic hinge in beam

$w_{wa}$  : web angles width

$\alpha$  : coefficient of thermal expansion

$\beta$ : parameter depending on geometry and material

$\Delta$  : beam axial deformation

$\Delta P_i$  : incremental axial force

$\Delta P_{i(\text{compression})}$  : incremental compressive axial force

$\Delta P_{i(\text{tension})}$  : incremental thermal tensile axial force

$\Delta T_i$  : temperature increment

$\Delta \theta_i$  : incremental connection rotation

$\Delta \theta_y$  : incremental connection rotation at connection yielding capacity

$\phi$  : geometry dependent factor

$\sigma_{avg}$  : average buckling stress

$\theta_{geom}$  : geometric angle between column flange and beam bottom flange

$\theta_i$  : total connection rotation

$\theta_{(T)}$  : connection rotation at every temperature



# CHAPTER I

## INTRODUCTION

Beam end framing steel connections are critical elements that transfer the floor load to columns or girders. Current design procedures account only for gravity loads on such connections. However, during a fire, large axial forces can be generated in steel beams and beam end connections [1]. At elevated temperatures, beams undergo restrained expansions creating compressive axial forces in the connection. Near the end of the heating phase of a fire, these axial forces become tensile and the beam sags. During the cooling phase, the tensile axial forces increase as the beam contracts. Furthermore, large rotational deformations develop in the connection due to thermal demands [2]. These large thermally induced axial forces, deformations, and rotations demands may result in failure of the connection during or after fire.

Steel connections are classified in three groups: rigid, partially restrained and pinned connections depending on their stiffness [3]. Top and seat angle connections were initially designed as pinned connections. Later on, their capability to resist moment allowed to design them also as partially restrained connections that restrain moment but allow some rotation [4]. As previously discussed, top and seat angle connections are designed to resist only gravity loads at ambient temperature; however, the flexural resistance of such connections cannot be ignored especially when subjected to fire [5].

Very few experimental studies were conducted to analyze the behavior of isolated and composite top and seat angle connections subjected to fire. The most important ones include the experiments conducted by Saedi and Yahyai [6] and Yuan et al. [7]. The effect of concrete slab on the behavior of such connections under fire was investigated by Yuan et al. [7]. It was concluded that the additional strength and stiffness provided by composite beam-slab significantly improves the behavior of beam-column connections subjected to fire loading. Also, Saedi and Yahyai [6] performed twelve experimental tests on top and seat angles with and without web angles subjected to elevated temperatures. It was concluded that the angle thickness, the bolt strength and the applied moment and forces are the main factors affecting the resistance of such connections. Furthermore, this study showed that tension bolt failure occurred thus depriving the use of full capacity of the remaining connection components. Also, Saedi and Yahyai [8] developed a series of FE models to reproduce the experimental temperature-rotation and moment-rotation response and failure modes. The failure modes were tension bolt yielding and fracture of top angle. A mechanical model was developed and validated against four of the specimens of this experiment [9]. The model predicted the temperature-rotation and moment-rotation response of isolated top and seat angle connections with and without web angles. Also, Pirmoz et al. [5] developed a mechanical model that predicts the behavior of such connections; however, the model was limited in predicting the stiffness of the top angle and tension bolts without including the stiffness contributions of other components such as column flange, column web, shear bolts and web angles. Reinoso et al. [10] proposed an analytical approach (based on the T-stub analogy) to predict the rotational stiffness of top and seat angle connections with double web angles. Also, Yuan et al. [7] and Yang et al.

[11] proposed mechanical models to predict the moment-rotation response of top and seat angle connections with and without web angles, respectively. The resistance of any connection can be determined by assembling the resistance of its different components as per Eurocode3 [3]. Previous studies were conducted to quantify the stiffness of different components of steel beam-column connections [2, 12, 13, 14, 15 and 16]. However, failure modes, forces, and deformations demands are still not well understood. Also, existing mechanical models did not include the effect of the beam on the connection response at elevated temperatures and did not predict the thermal axial forces and rotations of the beam-column connection assembly.

The goal of this paper is to develop a mechanical model that predicts the temperature-rotation and axial force-temperature of steel top and seat angle connections subjected to elevated temperatures. To achieve this purpose, FE models of top and seat angle connections at elevated temperatures are developed to reproduce the temperature-rotation and failure modes of experimental work available in the literature [6]. Furthermore, FE models of a connection assembly are also developed and used to conduct a parametric study to identify the key geometric parameters that affect the behavior of bolted top and seat angle connections during the heating and cooling stages of a fire. This includes load ratio, beam length, top-seat angle thickness, and gap distance. This study aims at providing a set of data to develop a mechanical model to account for the thermally-induced axial forces and deformations on these connections when exposed to fire. The proposed model is developed and validated against the results of this parametric study and experimental results available in the literature.

## CHAPTER II

### FE MODEL OF ISOLATED TOP AND SEAT ANGLE CONNECTION

#### **A. Development of the FE model**

FE model is developed in ABAQUS to reproduce the temperature-rotation response of an experimental work for validation purposes [6]. Figures 1(a) and 1(b) show the FE model of bolted top and seat angle connections with and without web angles, respectively.

#### ***1. Geometry of connection components***

The first specimen (denoted as Exp.1) consists of top and seat angles L6×4×5/8 in. (L150×100×15 mm) as used in the experiment. The second specimen (denoted as Exp.2) consists of top and seat angles L4×4×7/16 in. (L100×100×10 mm). The third and fourth specimens (Exp.1-w and Exp.2-w respectively) are similar to the first and second specimens having double web angles, 2L4×4×5/8 in. (2L100×100×15 mm). The angles are connected to W12×26 (IPE300) column and to W8×15 (IPE220) beam with 5/8 in. (16 mm) diameter bolts (M16) used for both tension and shear bolts. Details of the connection configuration can be found in the literature [6].

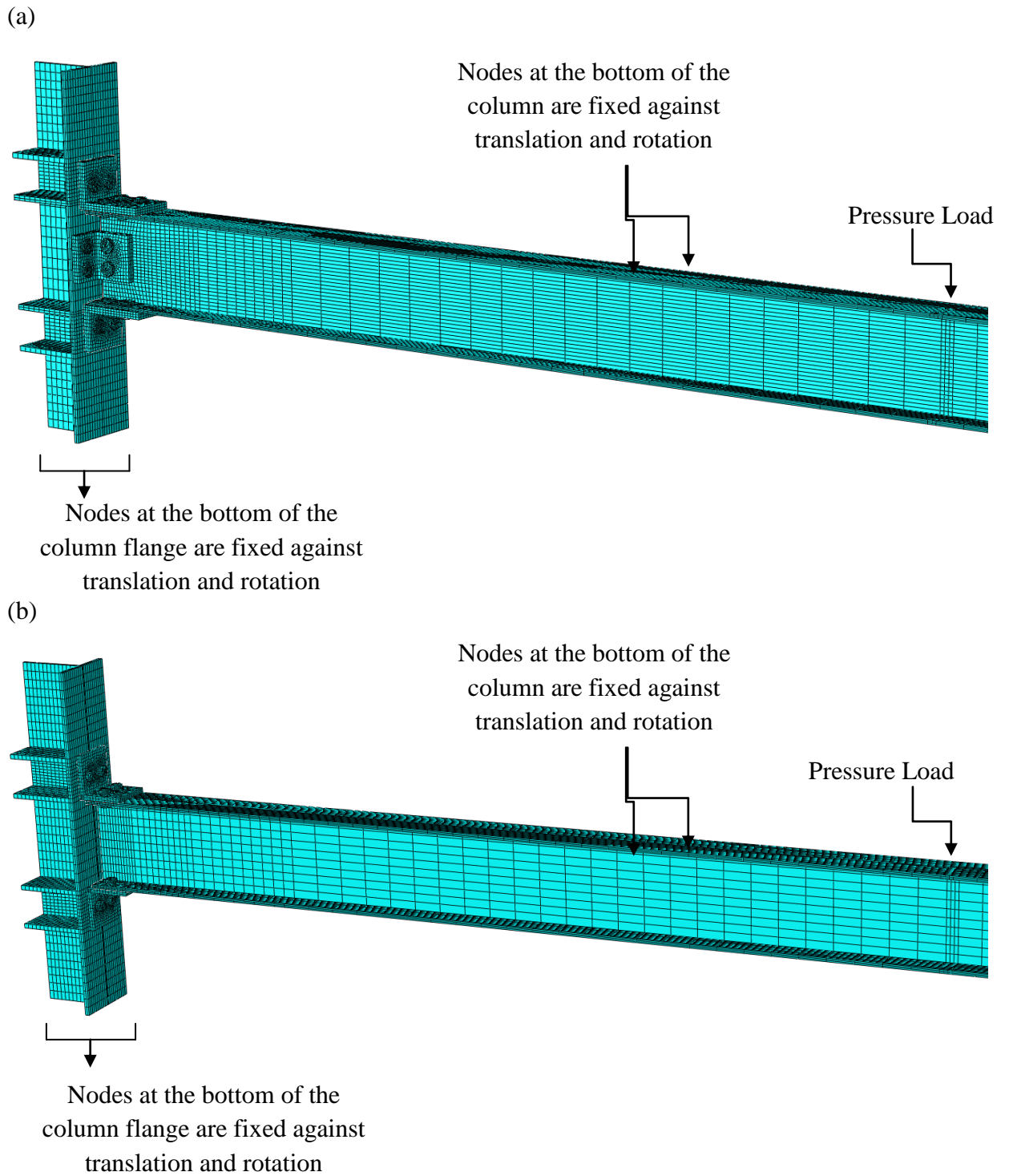


**Figure. 1.** Connection details in FE model: (a) Top and seat angle with web angles, (b) Top and seat angle without web angles

## ***2. Geometric and force boundary conditions***

All specimens are loaded in two steps. In the first step, tension and shear bolts are subjected to a pretension force. The pre-tensioning is modeled by applying a pressure on the nuts of the bolts equivalent to the minimum required pretension force specified in the AISC Specification [17]. In the second step, a concentrated load is applied at the tip of the beam. The loading is applied as a pressure on the beam at a distance of 79 in. (200 cm) away from the connection in accordance with the experiment [6].

Boundary conditions are applied on the system throughout the analysis as shown in Figs. 1(a) and 1(b). During all steps of the analysis, the beam is restrained from moving in the horizontal direction to prevent lateral torsional buckling. All nodes at the column bottom flange are assumed to be restrained against any translation and rotation and all nodes at the column top flange are free to move reflecting the experimental test set up [6, 8]. Note that, half the connection was modeled and symmetry was applied all along the length of the column to model the symmetry of the connection as shown in Figs. 1(a) and 1(b).

## ***3. Material Properties***

An idealized bilinear model is used for all steel materials. The mechanical properties of the beam, angles and column at ambient temperature used in the FE model are: the yield stress  $F_y = 34$  ksi (235 MPa), and the ultimate stress  $F_u = 61$  ksi (420 MPa). All bolts have a yield stress  $F_y$  of 107 ksi (740 MPa) and an ultimate stress  $F_u$  of 125 ksi (866 MPa). The mechanical properties of all structural material at elevated temperatures can be calculated using the retention factors proposed by Eurocode3 [19]. Note that the mechanical properties of all materials are in conformity with those specified in [5].

#### ***4. Model discretization***

Discretization of all the components of the connection model in ABAQUS is performed using C3D8-R (eight-node brick elements with reduced integration). The element type used in the simulations is chosen to accurately model the real behavior of the connection with reasonable accuracy and preventing shear locking problems. The mesh configuration is shown in Fig. 1. As noticed, at regions where failure is expected to occur (at the proximity of the connection), and at regions where stress is likely to concentrate (around bolt holes and at the point of application of the load) a finer mesh and a mapped mesh are adopted respectively in order to advance the accuracy of interpolations.

Surface-to-surface contact with a finite sliding coefficient is used to reproduce contact surfaces between the bolt shank, the angles, the beam and the column. This finite sliding is used to represent a friction coefficient of 0.25 as per Saedi and Yahyai [8]. The finite sliding allows separation, sliding, and rotation of the contact surfaces.

#### ***5. Analysis procedure***

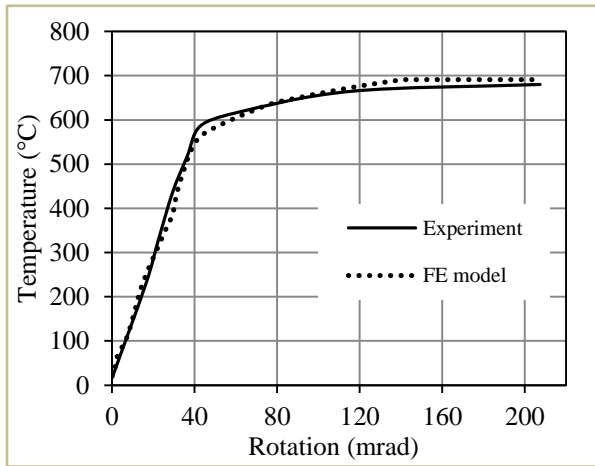
In order to predict the strength and behavior of top and seat angle connections with and without web angles exposed to fire, a transient temperature analysis is assumed in all ABAQUS models of the connection in compliance with the experiment [6]. The connection models are subjected to a concentrated gravity load applied at the tip of the beam. While keeping this load constant, the connection, as well as part of the column and beam at the proximity of the connection, is heated up until failure. Note that since material fracture is not considered in the analysis of the connection, post-ultimate response cannot be obtained. The objective is to identify the limit states in the loaded connection under fire loading.

## **B. Comparison of FE predictions with experiments**

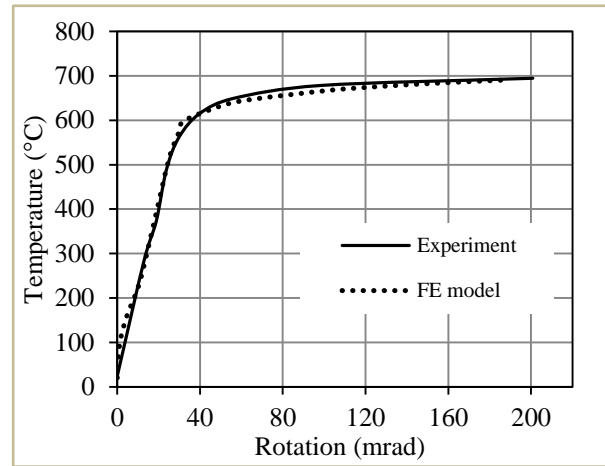
The capability of the ABAQUS model to predict the strength of top and seat angle with and without web angles under fire loading is validated against full scale tests [6]. Plots of temperature versus rotation of connection for both experimental and ABAQUS models are shown in Fig. 2. It can be seen that in all four specimens, the FE results are in good agreement with the experimental results. The FE models predict well the connection rotation at yield and plastic states, the connection behavior and failure modes. Both FE and experimental results show that for the same angle size, adding web angles will slightly delay failure of the connection as shown in Fig. 2. In both FE and experimental specimens, failure is governed by tension bolt failure (Exp.1 and Exp.1-w) and top angle leg failure (Exp.2 and Exp.2-w). Also, FE and experimental results show that using thinner angles reduces the capacity of the connection and the governing failure mode is top angle leg failure as shown in Fig. 3(a) and 3(b). The FE models of top and seat angle connections with and without web angles have been proven to be accurate in predicting the strength, failure mode, and rotation of such connections in fire. Thus, FE models can be used for developing the parametric study.



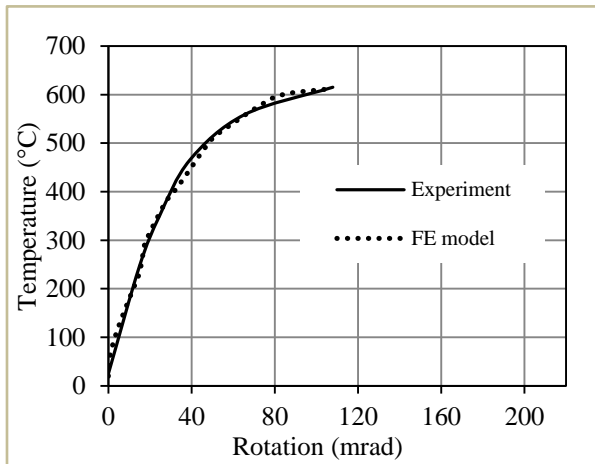
(a)



(b)



(c)



(d)

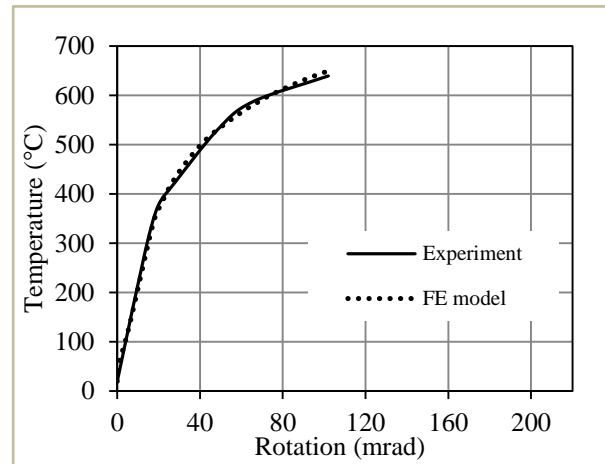
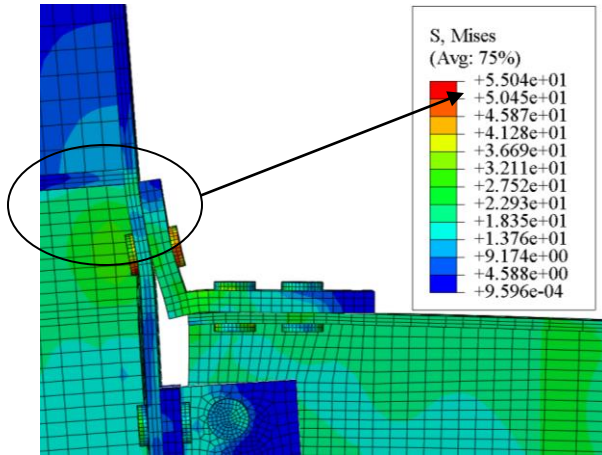


**Figure 2.** FE vs. Experiment: Temperature vs. rotation of connection: (a) Exp.1, (b) Exp.1-w, (c) Exp.2, (d) Exp.2-w.

(a)



(b)

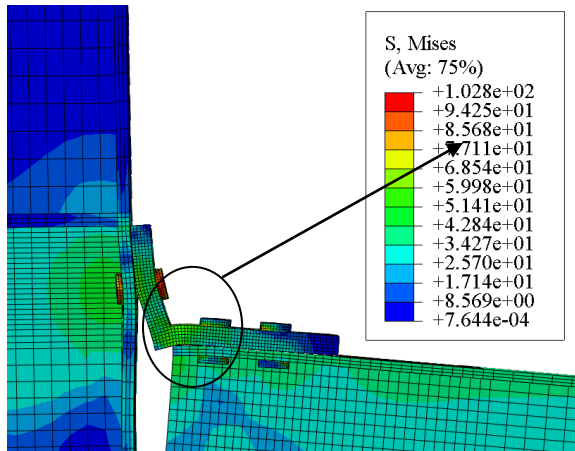


**Figure. 3.** Von Mises stress contours vs. experimental results: (a) Tension bolt failure (Exp.1 and Exp.1-w), (b) Top angle failure (Exp.2 and Exp.2-w).

## CHAPTER III

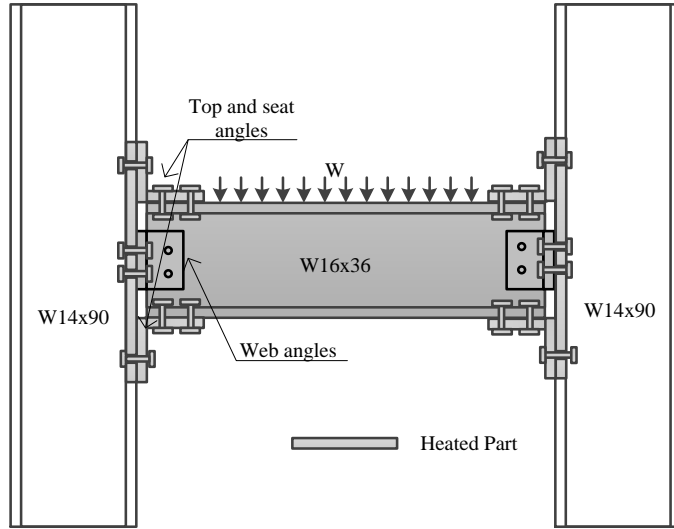
### TOP AND SEAT ANGLE CONNECTION ASSEMBLY: EVALUATIONS OF DEMAND

Top and seat angle connections are usually designed to resist gravity loading only at ambient temperature. When exposed to fire, demands on the connection increase because large axial forces develop in the beam and connection. Therefore, FE models of top and seat angle connection assemblies are developed in ABAQUS and used to conduct parametric studies on the behavior of beam-to-column top and seat angle connections subjected to fire. The main objective of these studies is to gain additional understanding of the key parameters that influence the performance of top and seat angles exposed fire. FE analysis is used since it is costly, time consuming and ineffective to perform experimental parametric studies. Note that the study has three main limitations: the connection performance after first fracture is not considered, the composite concrete floor system is not included in the models, and no creep effect is included in the analysis.

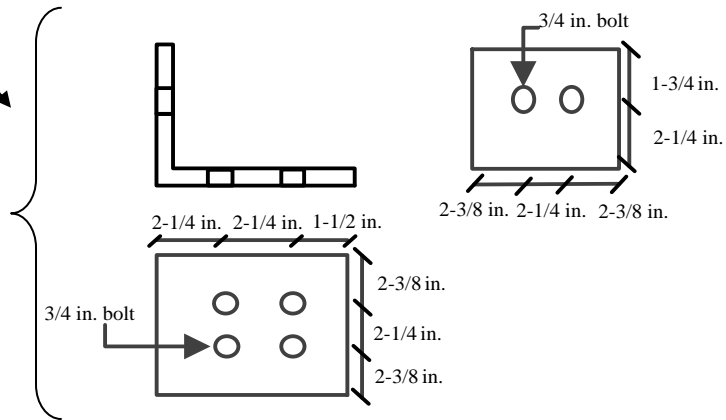
#### **A. Description of the connection assembly model**

A typical beam-to-column connection is designed to conduct the parametric study in conformity with the procedure proposed by Schippers [19]. A W16x36 is connected to a 10 ft. (3.05 m) long W14x90 column using bolted top and seat angles as shown in Fig. 4. Material properties of all steel components of the connection at ambient temperature used in the ABAQUS models are similar to the ones used by Hu and Engelhardt [20] in a previous study on shear tab connections. The structural bolts used in the FE model are ASTM A490. For elevated

temperature material, the retention factors proposed by Eurocode3 [18] are used to define the material properties of these bolts. As for the steel material of all other components of the top and seat angle connection, the retention factors proposed by Lee et al. [21] are used to define the elevated temperature material properties of this base material. The column is assumed to be pinned at both the top and bottom ends. The connection is designed to sustain a gravity load that produces a moment equal to the plastic moment capacity of the beam. While keeping the load constant, a temperature gradient is applied to the connection making the analysis transient. The beam, the top and seat angle, the web angles if present, and part of the column which is in contact with the connection were heated. The remaining part of the column is assumed to be insulated. The temperature is assumed to increase linearly with time and to be uniformly distributed in the heated parts of the structure [22]. The temperature is increased to 650 °C and then cooled down to 20 °C. Due to perfect symmetry of connection assembly, symmetry is applied to the beam flange and web at mid span section.



(L6×4×7/8)  
Top and seat angles



(L5×5×1/2)  
Web angles

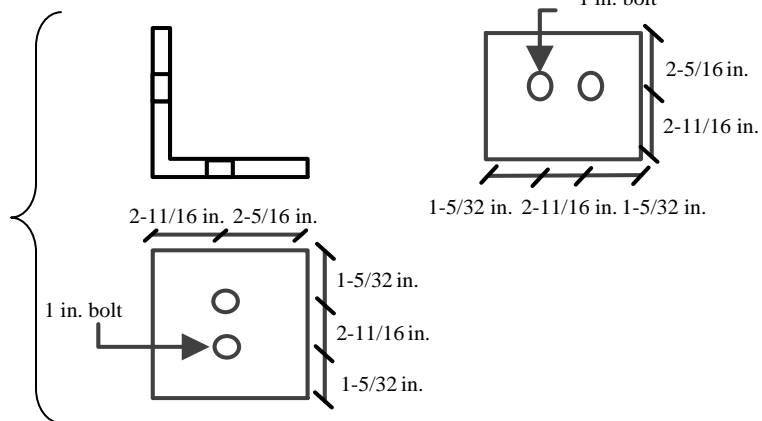


**Figure. 4.** Layout of connection assemblies used in parametric study.

## B. Effect of key parameters and connection details

Several key parameters including load ratio, beam length, top and seat angle thickness, and gap distance are examined. All cases analyzed in this parametric study are listed in Table 1.

**Table 1.** Parametric study cases using FE modeling.

Case	Column section	Beam section	Beam length (ft.)	Load ratio	Angle thickness (in.)	Gap distance	Web angles
1	W 14×90	W 16×36	30	0.25M <sub>p</sub>	7/8	0.50	No
2			30	0.25M <sub>p</sub>	7/8	0.50	Yes
3			30	0.50M <sub>p</sub>	7/8	0.50	No
4			30	0.50M <sub>p</sub>	7/8	0.50	Yes
5			30	1.00M <sub>p</sub>	7/8	0.50	No
6			30	1.00M <sub>p</sub>	7/8	0.50	Yes
7			20	0.33M <sub>p</sub>	7/8	0.50	No
8			20	0.33M <sub>p</sub>	7/8	0.50	Yes
9			30	0.33M <sub>p</sub>	7/8	0.50	No
10			30	0.33M <sub>p</sub>	7/8	0.50	Yes
11			40	0.33M <sub>p</sub>	7/8	0.50	No
12			40	0.33M <sub>p</sub>	7/8	0.50	Yes
13			30	0.50M <sub>p</sub>	1	0.50	No
14			30	0.50M <sub>p</sub>	1	0.50	Yes
15			30	0.50M <sub>p</sub>	7/8	1.00	No
16			30	0.50M <sub>p</sub>	7/8	1.00	Yes

### 1. Load ratio

The load ratio is the maximum moment developed at the beam mid-span divided by the nominal plastic moment capacity of the beam section. For the load ratio parameter, the length of the beam was taken to be 30 ft. (9.15 m). Three load ratios are analyzed: 0.25, 0.50, and 1.00. Figure 5(a) shows that when the load ratio is increased, the maximum compressive axial force on the connection is reduced. The beam starts yielding and cannot develop additional thermally induced compressive axial forces. For the three load ratios, failure of shear bolts, indicated by von Mises stress distribution, occurred around 570°C. Figure 5(b) shows that as the load ratio increases, the beam rotation increases. This is due to the plastic hinge that starts developing in

the beam. For the same load ratio, adding web angles slightly increases the maximum compressive axial force and the initial connection stiffness (Fig. 5(c)).

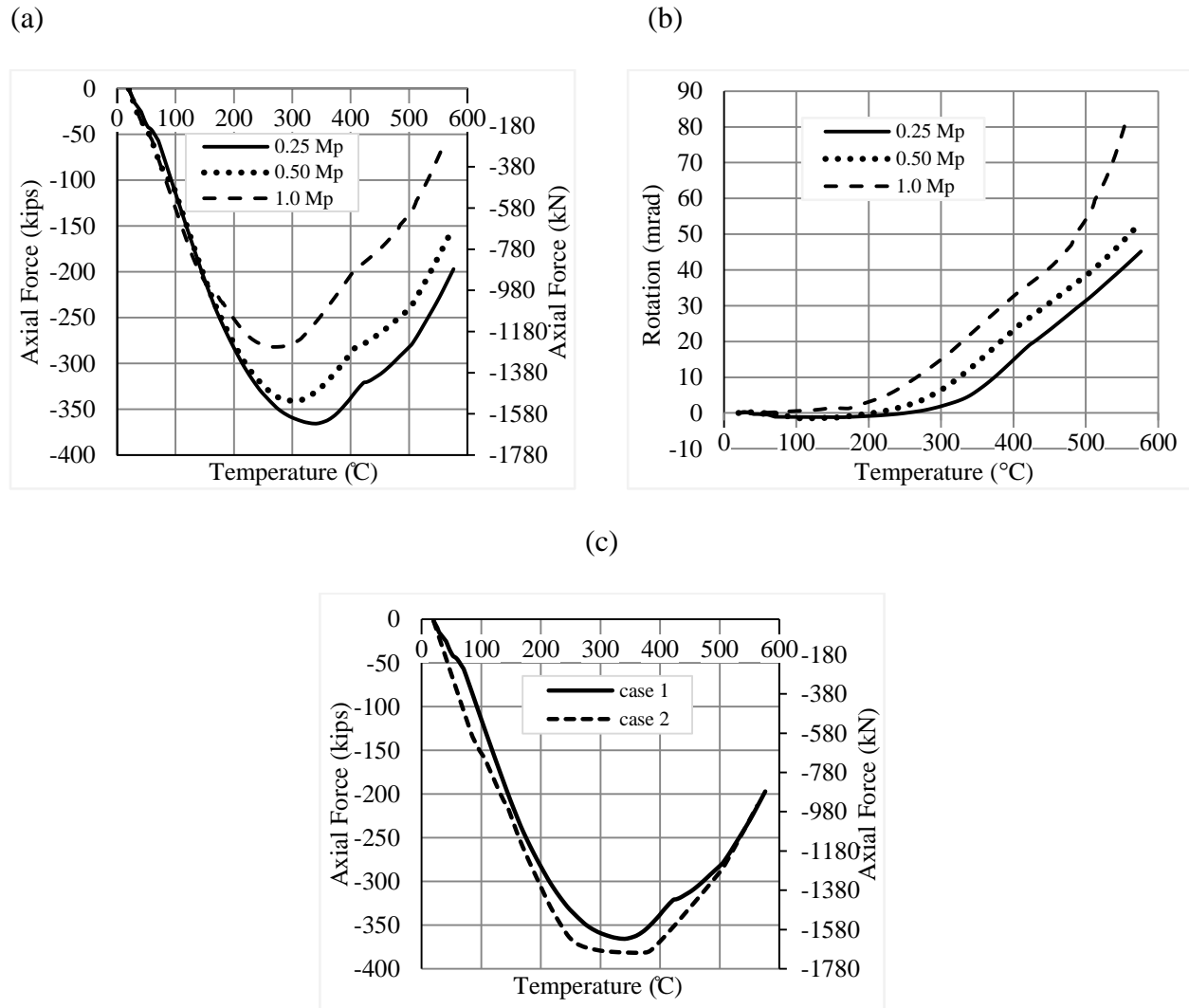


**Figure 5.** (a) Axial force for varying load ratio, (b) Connection Rotation for varying load ratio, (c) Axial force comparison with and without web angles (case 1 vs. case 2).

## 2. Beam length

Beam length effect on the connection behavior is analyzed. Three typical beam lengths are selected for analysis: 20 ft (6.10 m), 30 ft (9.15 m), and 40 ft (12.20 m). In all cases, the load is chosen to be 1/3 of the full beam plastic moment capacity. Figure 6(a) shows that the maximum axial compressive force on the connection for longer beams occurs at a lower

temperature. The maximum compressive axial force increases when the beam length increases from 20ft to 30ft, as the beam length is proportional to the axial force, but decreases when the beam length increases to 40 ft. This is due to the fact that the column flange buckles and then yields early in the heating stage when a 40 ft. beam is used. From Fig. 6(b), it is found that the longest beam has the lowest rotational stiffness producing the highest connection rotation. Adding double web angles increases the maximum compressive axial force and initial connection stiffness (Fig. 6(c)).

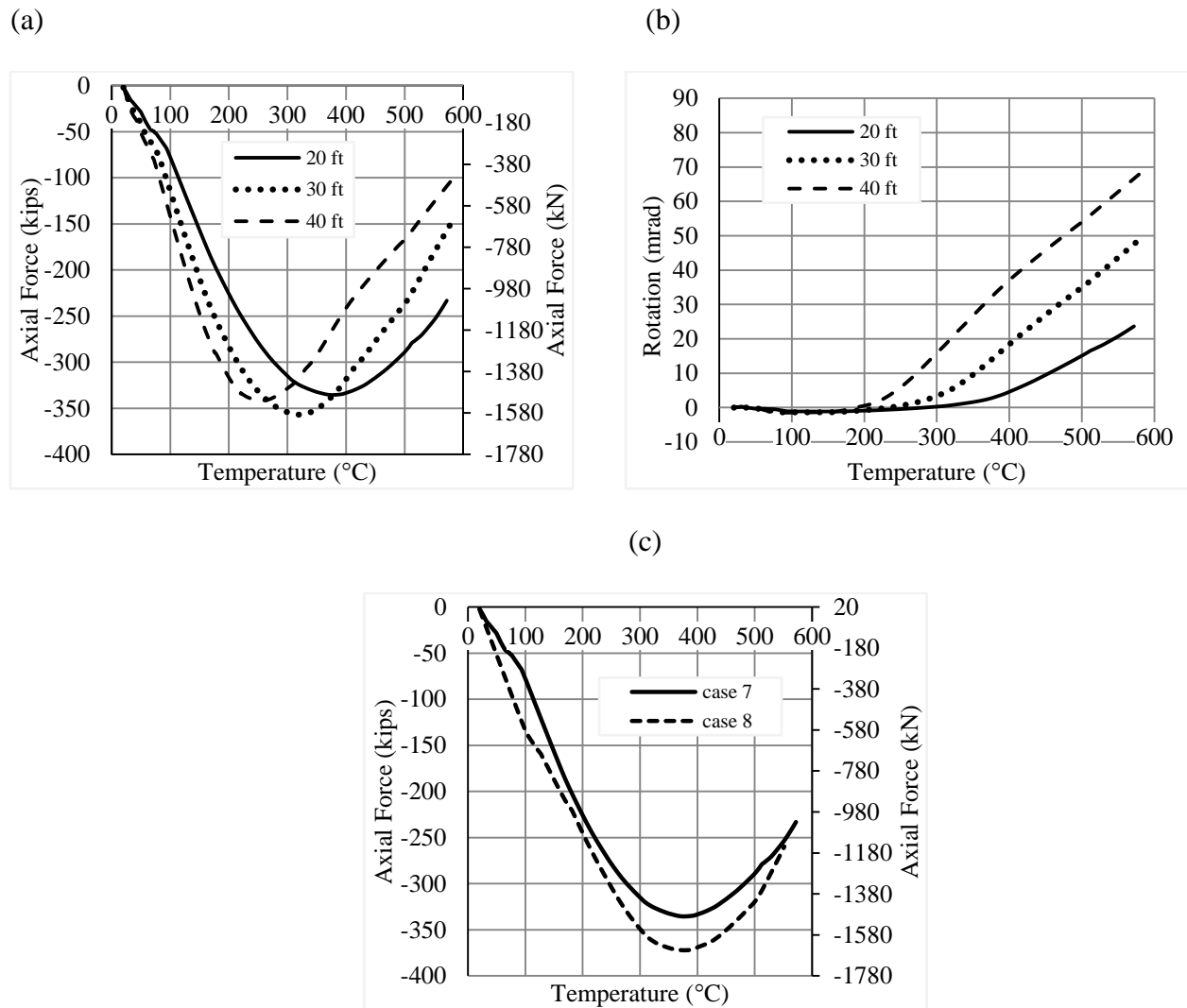


**Figure 6.** (a) Axial force for varying beam length, (b) Connection Rotation for varying beam length, (c) Axial force comparison with and without web angles (case 7 vs. case 8).



### 3. Top and Seat Angle thickness

Angles thicknesses of 7/8 in. (22 mm) and 1.0 in. (25 mm) are considered to investigate the effect of the angle thickness on the behavior of the connection. A 30 ft (9.15 m) beam is used in the analysis with a load ratio of 0.50. The beam axial force decreases as the angle thickness increases (Fig. 7(a)). The failure temperature increases from 570°C to 600°C as the angle thickness increases. However, the connection stiffness remains unchanged (Fig. 7(b)). For the same angle thickness, adding web angles increases the compressive axial force and initial connection stiffness (Fig. 7(c)).

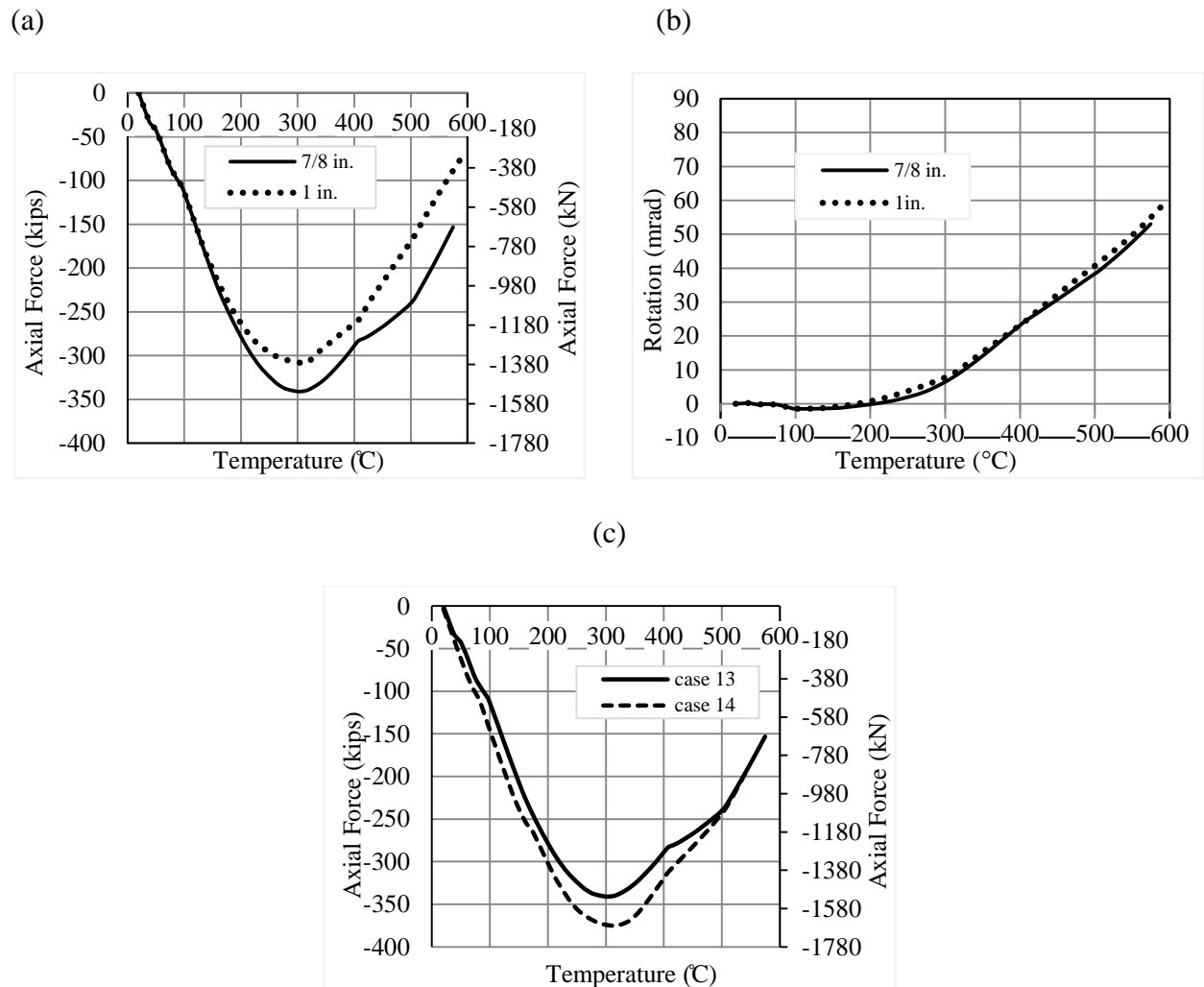


**Figure 7.** (a) Axial force for varying angle thickness, (b) Rotation for varying angle thickness, (c) Axial force comparison with and without web angles (case 13 vs. case 14).

#### ***4. Gap distance***

Gap distance is defined as the distance between column and beam flanges. When the connection rotates significantly, the beam bottom flange may come into contact with the column changing the response of the connection to fire. Two cases are considered: 1/2 in. (12.25 mm) gap distance and 1.0 in. (25.4 mm) gap distance. A 30 ft (9.15 m) beam is used with a load ratio of 0.50. The compressive axial force decreases as the gap distance increases (Fig. 8(a)). The moment applied at the face of the column is proportional to the gap distance. The bottom beam flange yields earlier, thus the maximum compressive axial force decreases. The connection rotation and failure temperature remain unchanged when the gap increases (Fig. 8(b)). For the same gap distance, adding web angles increases the connection initial stiffness and maximum compressive axial force (Fig. 8(c)).

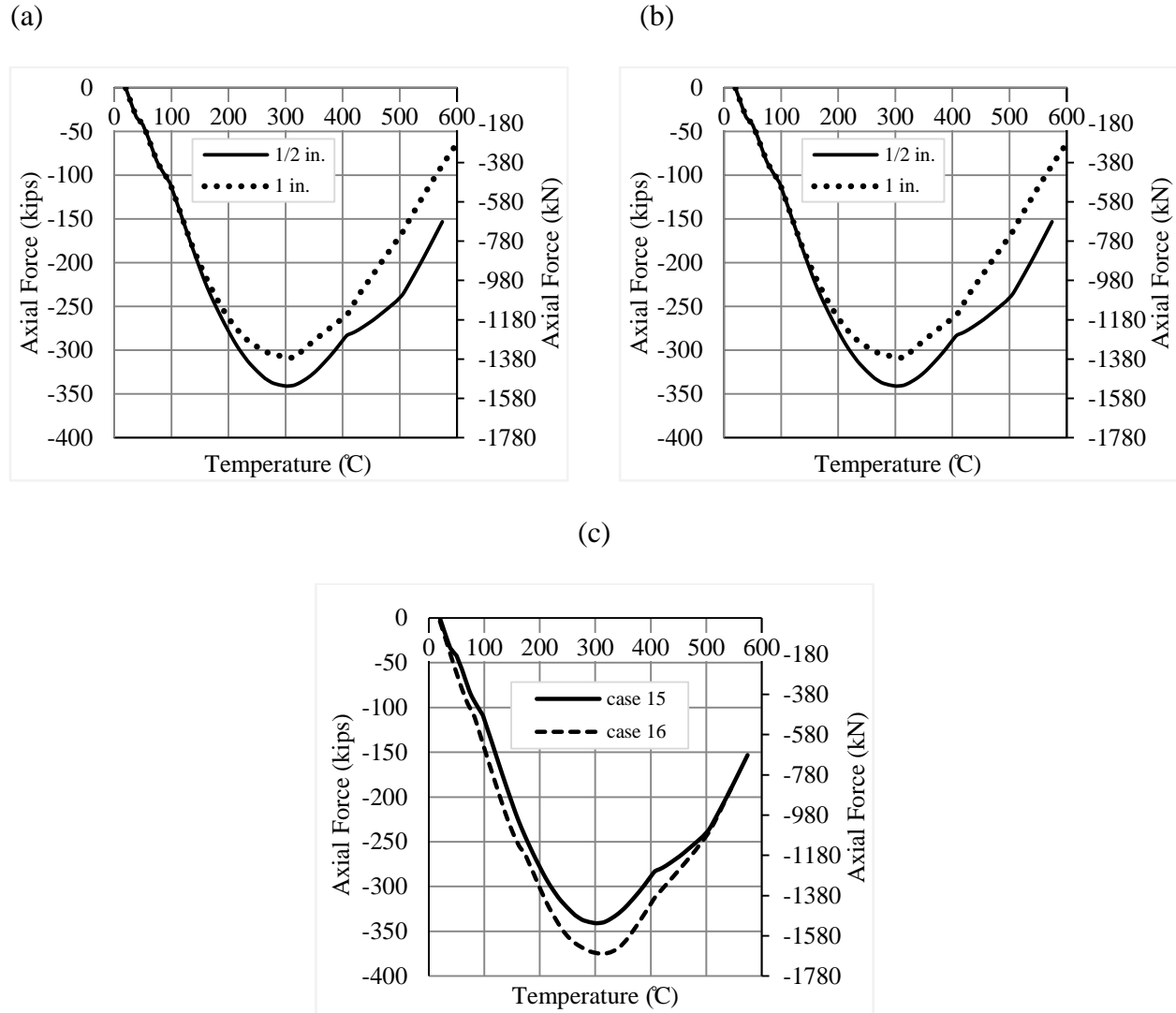


**Figure 8.** (a) Axial force for varying gap distance, (b) Rotation for varying gap distance, (c) Axial force comparison with and without web angles (case 15 vs. case 16).

A summary of all FE results of this parametric study can be found in Table 2. The failure mode of all cases studied is shown to be shear bolt failure. Table 2 shows the temperature at failure, maximum compressive axial force, maximum rotation, and the percentage difference with respect to top and seat angle connection with web angles. As shown in Table 2, web angles increase the maximum compressive axial force in cases 11, 13, and 15 and decrease the maximum rotation in cases 13, and 15, and has no significant effect on the failure temperature.

**Table 2.** FE results comparison of top and seat angle connection with and without web angles.

Case	Failure mode	Temperature at failure (°C)		Maximum compressive axial force (kips)		Maximum rotation (mrad)	
		Temperature (°C)	% difference (without vs. with web angle)	Axial force (kips)	% difference (without vs. with web angle)	Rotation (mrad)	% difference (without vs. with web angle)
2	Top and seat shear bolt	562	-	382.00	-	41.00	-
1		576	2.49%	366.00	-4.19%	45.00	9.76%
4		546	-	375.00	-	51.00	-
3		574	5.13%	341.00	20.92%	53.00	3.92%
6		537	-	282.00	-	76.00	-
5		557	3.72%	282.00	0.00%	83.00	9.21%
8		552	-	372.00	-	24.00	-
7		572	3.62%	336.00	-9.68%	24.00	0.00%
10		577	-	382.00	-	47.00	-
9		583	1.04%	357.00	-6.54%	49.00	4.49%
12		556	-	384.00	-	63.00	-
11		586	5.40%	342.00	-10.94%	69.00	9.52%
14		547	-	378.00	-	49.00	-
13		596	8.96%	309.00	-18.25%	60.00	22.45%
16		542	-	375.00	-	49.00	-
15	581	7.20%	338.00	-10.95%	55.00	12.24%	

## CHAPTER IV

### MECHANICAL MODEL

A mechanical model is developed to predict the axial force-temperature and rotation of top and seat angle connections with and without web angles at elevated temperatures.

The proposed model consists of multi-linear and nonlinear springs that predict each component stiffness, strength and rotation. The proposed model, unlike previous ones available in literature [5,9] is able to predict both the elastic and plastic states of the connection including all components contribution. Also, the proposed model includes the effect of thermal axial restraint forces in the connection response of typical steel frames. It is important to note that prying effect on top and seat angles was not included in the formulation, and that the model is applicable only for slender beam flanges as defined in Selamet and Garlock [23].

The connection contribution includes column web and flange stiffnesses, top angle horizontal and vertical legs stiffnesses, tension and shear bolts stiffnesses, and web angle stiffness as shown in Fig. 7(a). Each component of the connection is modeled using a spring stiffness based on its behavioral characteristics.

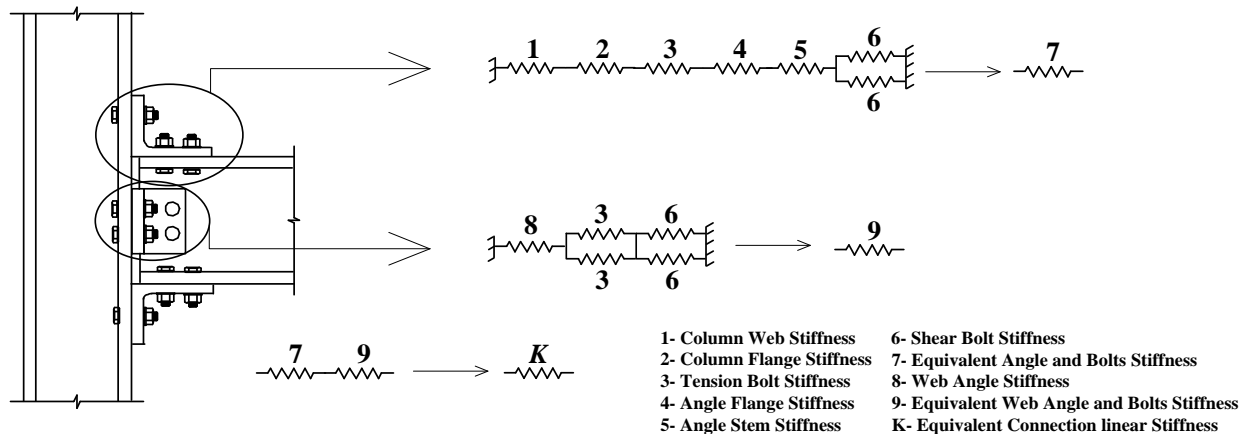


**Figure. 9.** Mechanical model: Components stiffnesses.

## A. Component stiffness

### 1. Column web

The column web stiffness,  $K_{cw}$ , acting in tension can be computed as per Eurocode 3 part 1.8 [3] and is defined as:

$$K_{cw} = \frac{0.7b_{eff-cw}t_{cw}}{d_{cw}} E \quad (1)$$

where  $t_{cw}$  is the thickness of column web,  $d_{cw}$  is the effective depth of column web

( $d_{cw} = d_c - 2k_{des}$ , where  $d_c$  is the depth of the column, and  $k_{des}$  is the design fillet size of the column),  $b_{eff-cw}$  is the effective length of column web and is assumed to be the effective length of an equivalent T-stub representing the column flange ( $b_{eff-cw} = 4m + 1.25e$ , where  $m$  is the clear distance between the angle fillet and the bolt centerline, and  $e$  is the distance between the bolt centerline and the upper edge of the angle as shown in Fig. 10(a)), and  $E$  is the modulus of elasticity of the component.

### 2. Column flange

The flexural stiffness of the column flange,  $K_{cf}$ , is defined as per [3]:

$$K_{cf} = \frac{0.9l_{eff-cf}t_{cf}^3}{m^3} E \quad (2)$$

where  $t_{cf}$  is the thickness of column flange, and  $l_{eff-cf}$  is the effective length of column flange defined to be equal to the effective length of equivalent T-stub representing the column flange ( $l_{eff-cf} = 4m + 1.25e$ ) (Fig. 10(a)).

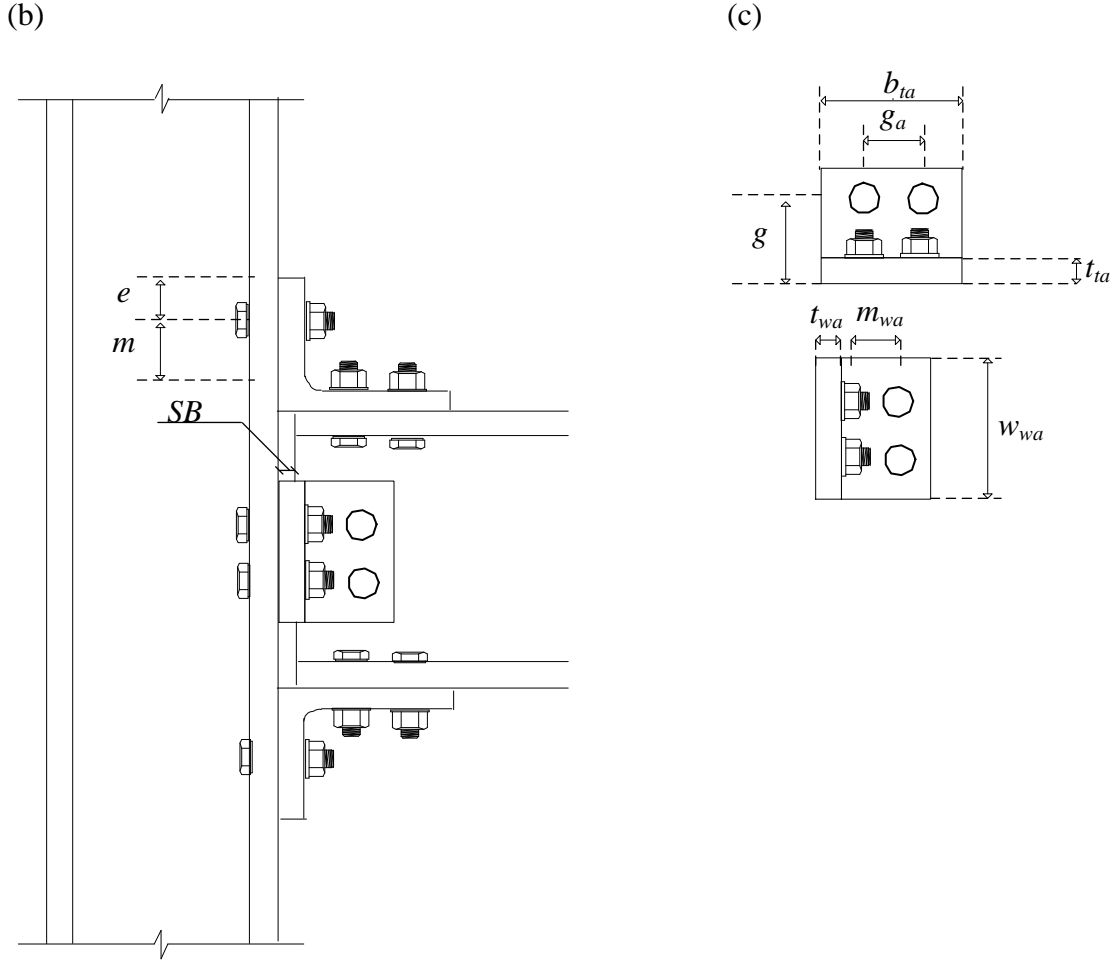


**Figure 10.** Mechanical model: (a) Connection, (b) Top and seat angle, web angle.

### 3. Top angle vertical leg

The stiffness of top angle vertical leg,  $K_{tav}$ , in bending is defined as per Pirmoz et al. [5]:

$$K_{tav} = \frac{3I_a}{(g - t_{ta})^3} E \quad (3)$$

where  $t_{ta}$  is the thickness of top angle,  $g$  is the gage distance, and  $I_a$  is the moment of inertia of the angle leg ( $I_a = b_{ta}t_{ta}^3 / 12$ , and  $b_{ta}$  is the width of top angle (Fig. 10(b)).

#### 4. Top angle horizontal leg

The top angle horizontal leg stiffness,  $K_{tah}$ , acting in tension can be written as per Pietrapertozza and Jaspart [15]:

$$K_{tah} = \frac{b_{ta} t_{ta}}{g} E \quad (4)$$

#### 5. Tension bolts

The tension bolt stiffness,  $K_{tb}$ , is defined as per [5]:

$$K_{tb} = \frac{n_{tb} I_{bolt}}{L_b^3} E \quad (5)$$

where  $I_{bolt}$  is the moment of inertia of tension bolt ( $I_{bolt} = \pi d_b^4 / 32$ , and  $d_b$  is the diameter of bolt),  $n_{tb}$  is the number of tension bolts, and  $L_b$  is the tension bolt shank length.

#### 6. Shear bolts

The shear bolt stiffness,  $K_{sb}$ , can be written as follows:

$$K_{sb} = 32 n_{sb} (0.6 F_{ub}) \left( \frac{\pi}{4} d_b^2 \right) \quad (\text{US}) \quad (6a)$$

$$K_{sb} = 1.26 n_{sb} (0.6 F_{ub}) \left( \frac{\pi}{4} d_b^2 \right) \quad (\text{SI}) \quad (6b)$$

where  $F_{ub}$  is the ultimate strength of bolts, and  $n_{sb}$  is the number of shear bolts.

Note that Eq. 6(a) is for US system ( $F_{ub}$  in ksi and  $d_b$  in inches), and Eq. 6(b) is for metric system ( $F_{ub}$  in MPa and  $d_b$  in mm).



## 7. Web angles

The web angles stiffness,  $K_{wa}$ , is defined as per Yahyai et al. [9]:

$$K_{wa} = \frac{0.5b_{eff-wa}t_{wa}^3}{m_{wa}^3} \left(\frac{4}{7}\right)\phi E \quad (7)$$

where  $t_{wa}$  is the thickness of web angle,  $m_{wa}$  is the clear distance between the angle fillet and the bolt centerline (Fig. 10(b)), and  $b_{eff-wa}$  and  $\phi$  are the effective length of web angles and geometry dependent factor, respectively as defined in [9].

## B. Equivalent connection stiffness

An equivalent spring stiffness,  $K$ , is defined for the connection and can be determined by assembling stiffnesses of the connection components as shown in Fig. 9.

To compute the connection rotation, an equivalent rotational stiffness,  $K_{rot}$ , is needed to be determined as per [9]:

$$K_{rot} = Kh^2 \quad (8)$$

where  $h$  is the distance between the equivalent spring,  $K$ , and the connection center of rotation (beam bottom flange) as shown in Fig. 11 and can be computed as follows:

$$h = \frac{\sum K_i h_i^2}{\sum K_i h_i} \quad (9)$$

where  $K_i$  is the stiffness of each component, and  $h_i$  is the distance from the component under consideration to the beam bottom flange (center of rotation) (Fig. 11) (i.e.  $h_i$  is  $h_{cw}$ : the distance from column web center to beam bottom flange, and  $h_i$  is  $h_{cf}$ : the distance from column flange

center to beam bottom flange, etc...). The subscript  $i$  represents connection components contributing to the connection equivalent spring (see Fig. 11).

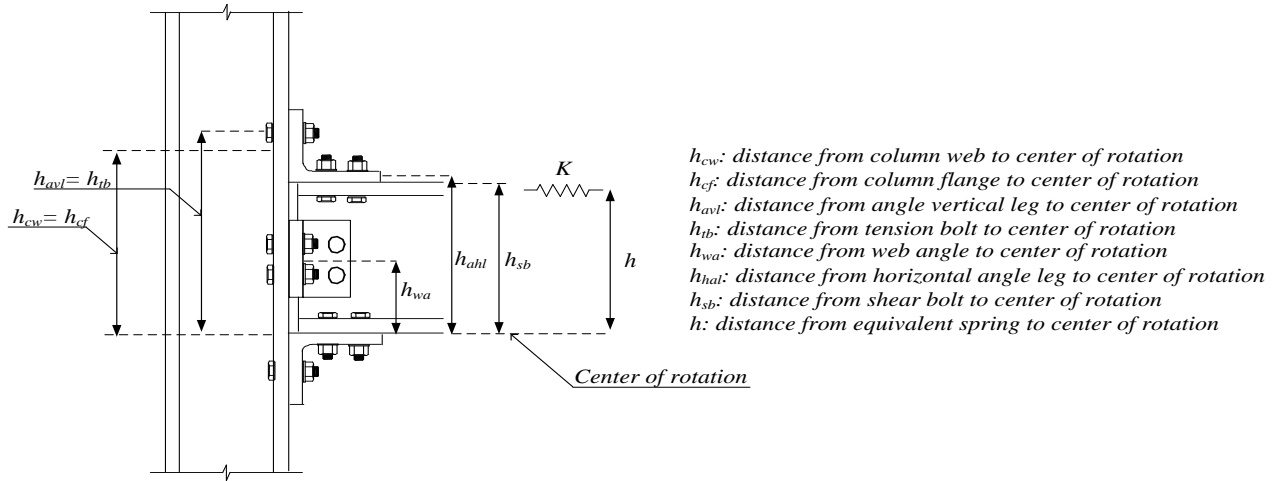


**Figure. 11.** Connection detailing.

### C. Connection rotation

The yielding and plastic moment capacities ( $M_y$  and  $M_p$ , respectively) are needed to be determined in order to predict the connection temperature-rotation response. The connection plastic moment capacity,  $M_p$ , can be written as a function of the top angle plastic moment capacity,  $M_{p-angle}$  [5]:

$$M_p = \frac{\beta M_{p-angle}}{g} h_b \quad (10)$$

where  $\beta$  is defined as a parameter depending on the geometry and material and can be found in [9], and  $h_b$  is the beam depth.

The connection yielding moment capacity,  $M_y$ , can be written as a function of  $M_p$  [5]:

$$M_y = \frac{M_p}{1.5} \quad (11)$$

The connection temperature-rotation at every temperature increment,  $\theta_{(T)}$ , is determined by assembling a stiffness matrix for the system shown in Fig. 12. Using direct stiffness method the connection-beam rotation, at node 2, in function of the temperature  $T$ , can be calculated as follows:

$$\theta_{(T)} = \frac{M_{(T)}}{K_{rot} + \frac{4E_b I_b}{L}} \quad (12)$$

where  $E_b$  is the modulus of elasticity of the beam,  $L$  is the beam length,  $I_b$  is the moment of inertia of the beam, and  $M_{(T)}$  is the applied moment on the connection in function of  $T$ .



**Figure. 12.** Equivalent rotational system

The temperature-rotation response of the connection is determined using an incremental analysis technique.  $K_{rot}$ ,  $M_y$ , and  $M_p$  are computed at every temperature increment step,  $\Delta T_i$ .

The pre-yielding incremental connection rotation,  $\Delta\theta_i$ , at every  $\Delta T_i$ , can be calculated as follows:

$$\Delta\theta_i = \frac{M_y}{K_{rot} \frac{M_{app}}{M_y} + \frac{4E_b I_b}{L}} \quad (13)$$

where  $M_{app}$  is the constant applied moment on the beam due to gravity load.

The total connection rotation,  $\theta_i$  at the  $i^{th}$  step can be calculated by adding the incremental connection rotation to the previous step:

$$\theta_i = \theta_{(i-1)} + \Delta\theta_i \quad (14)$$

where  $\theta_{i-1}$  is the total connection rotation at the  $(i-1)^{th}$  step.

When the connection reaches its yielding capacity,  $M_y$ , the post-yielding incremental connection rotation,  $\Delta\theta_i$  becomes:

$$\Delta\theta_i = \Delta\theta_y + \frac{M_p}{K_{rot} \frac{M_{app}}{M_p} + \frac{4E_b I_b}{L}} \quad (15)$$

where  $\Delta\theta_y$  is the incremental connection rotation at connection yielding capacity, and can be calculated using Eq.(13) by replacing  $M_{app}$  by  $M_y$ .

### ***1. Connection failure modes***

The proposed model is able to predict the following failure modes: top angle leg failure, tension bolt and shear bolt failure. The applied force on each component is determined and compared with its corresponding capacity (angle gross section yielding, tension bolt failure and shear bolt failure).

The applied force on top angle,  $P_{ta}$ , can be calculated as follows:

$$P_{ta} = \frac{M_{app}}{h_b + t_{ta}} \quad (16)$$

Assuming no prying effect, the applied force on the tension bolt,  $P_{tb}$ :

$$P_{tb} = \frac{M_{app}}{h_b + 2g} \quad (17)$$

The applied force on the shear bolt,  $P_{sb}$  :

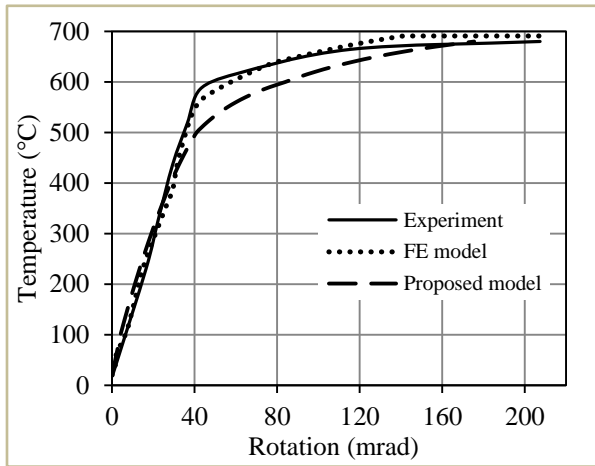
$$P_{sb} = \frac{M_{app}}{h_b} \quad (18)$$

The governing failure mode is the minimum of Eqs. (16), (17), and (18).

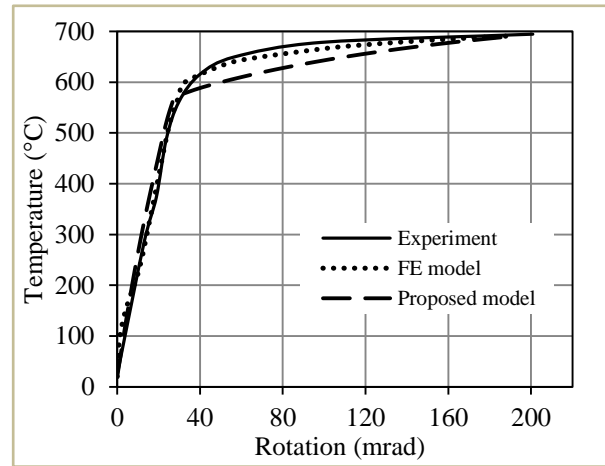
## ***2. Model performance***

The performance of the proposed mechanical model is validated by comparing the model predictions with the experimental results [5] and FE simulations. Figure 13 shows the temperature-rotation response of four top and seat angle connections. The results show acceptable agreement when compared with experimental and FE results. The model is able to predict both the elastic and plastic stiffnesses of the connection. Also, it predicts the connection failure mode which is tension bolt failure for both Exp.1 and Exp.1-w (Fig. 3(a)), and top angle leg failure for both Exp.2 and Exp.2-w (Fig.3(b)). Table 3 shows a comparison of the temperature at failure and the maximum rotation between experimental, FE and mechanical model results for the four cases studied. It can be seen from Table 3 that the percentage difference between the proposed model and FE and experimental results is considered acceptable.

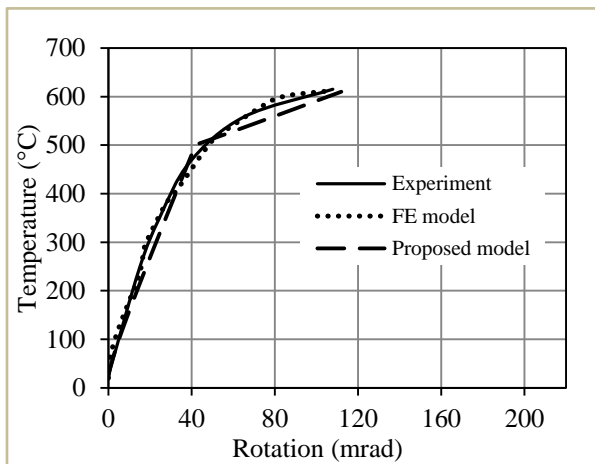
(a)



(b)



(c)



(d)

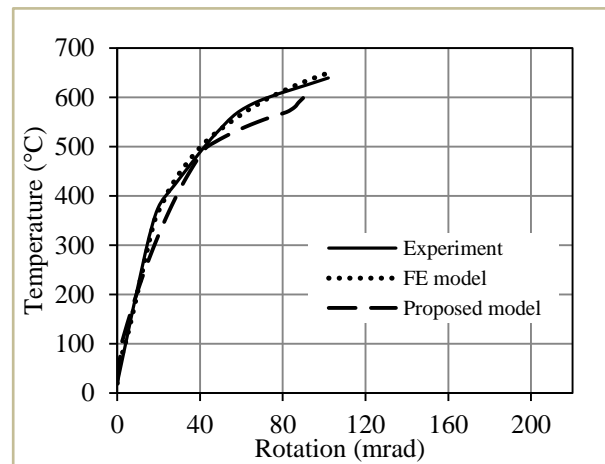


**Figure. 13.** Proposed model vs. FE vs. Experiment: Temperature vs. rotation of connection: (a) Exp.1, (b) Exp.1-w, (c) Exp.2, (d) Exp.2-w.

**Table. 3.** Experiment vs. FE vs. proposed model results of top and seat angle connection.

		Failure mode	Temperature at failure (°C)		Maximum rotation (mrad)	
			Temperature (°C)	% difference (model and FE vs. experiment)	Rotation (mrad)	% difference (model and FE vs. experiment)
Exp.1	Experimental	Tension bolt	694	-	201.00	-
	FE	Tension bolt	691	-0.43%	191.00	-4.98%
	Mechanical model	Tension bolt	690	-0.58%	189.00	-5.97%
Exp.1-w	Experimental	Tension bolt	680	-	207.00	-
	FE	Tension bolt	690	1.47%	207.00	0.00%
	Mechanical model	Tension bolt	680	0.00%	198.00	-4.35%
Exp.2	Experimental	Top angle	615	-	108.00	-
	FE	Top angle	612	-0.49%	107.00	-0.93%
	Mechanical model	Top angle	620	0.81%	102.00	-5.56%
Exp.2-w	Experimental	Top angle	640	-	102.00	-
	FE	Top angle	650	1.56%	103.00	0.98%
	Mechanical model	Top angle	650	1.56%	104.00	1.96%

#### D. Beam-column connection thermal axial force

The proposed model includes the effect of the beam to predict axial force demand at elevated temperatures.

Beams undergo restrained expansions resulting in compressive axial forces in the connection during the heating phase of a fire. Later in the heating phase, tensile axial forces start to develop. The proposed model predicts the thermally induced compressive and tensile axial forces. A stiffness matrix is assembled for the system shown in Fig. 14 to determine the axial forces developed. Using direct stiffness method, the incremental axial forces at every increase in temperature  $\Delta T$  can be calculated as follows:

$$\Delta P_i = K\Delta = \frac{KE_b A_b \alpha \Delta T}{\left(\frac{E_b A_b}{L} + K\right)} \quad (19)$$

where  $A_b$  is the beam area contributing to the thermal induced axial force,  $\Delta$  is the beam axial deformation,  $\alpha$  is the coefficient of thermal expansion, and  $\Delta T$  is the temperature increment at every  $10^\circ C$ .

The total axial force at every temperature increment can be calculated by adding the incremental axial force to the previous step axial force:

$$P_i = P_{(i-1)} + \Delta P_i \quad (20)$$

where  $P_i$  is the total axial force at the  $i^{th}$  step and  $P_{i-1}$  is the total axial force at the  $(i-1)^{th}$  step.

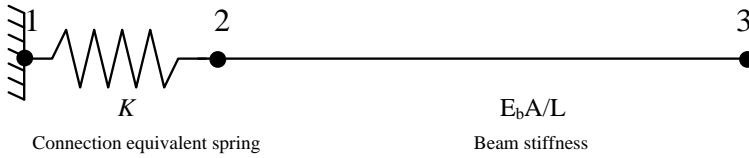


**Figure. 14.** Equivalent linear system.

### 1. Behavioral characteristics of top and seat angle connections

The proposed model is divided into ten stages. Different limit states indicate the end of one stage and the beginning of the next one until failure occurs.

#### a. Initial stage

The restrained top and bottom flanges of the beam develop compressive axial forces.

Therefore, only the beam top and bottom flanges are included in the formulation of the incremental compressive axial force:

$$\Delta P_{i(\text{compression})} = \frac{KE_b 2b_f t_f \alpha \Delta T}{\left(\frac{E_b 2b_f t_f}{L} + K\right)} \quad (21)$$



where  $b_f$  is the beam flange width and  $t_f$  is the beam flange thickness.

b. Stage 1: slip

As the temperature increases, compressive axial forces in the connection and beam increase until slip occurs. The axial deformation,  $\Delta_i$ , can be calculated as follows:

$$\Delta_i = \frac{P_i}{K} \quad (22)$$

During slip, the top angle develops tensile axial forces counteracting the compressive axial forces and therefore the incremental compressive axial force,  $\Delta P_{i(\text{compression})}$  becomes:

$$\Delta P_{i(\text{compression})} = \frac{KE_b 2b_f t_f \alpha \Delta T}{\left(\frac{E_b 2b_f t_f}{L} + K\right)} - \frac{KE_b t_a g_a \alpha \Delta T}{\left(\frac{E_b t_a g_a}{L} + K\right)} \quad (23)$$

where  $g_a$  is the gage distance between bolt holes in angle shown in Fig. 10(b).

As temperature increases, the thermal compressive axial force in the angle ( $P_{ca} = P_i / 2$ ) exceeds the external applied tensile force due to gravity loads (Eq. (16)). Thus, the angle cannot develop additional tensile axial forces and does not contribute to  $\Delta P_{i(\text{compression})}$  and  $\Delta P_{i(\text{compression})}$  is calculated using Eq. (21).

c. Stage 2: top beam flange yielding

The restrained beam flanges develop compressive axial forces until the top beam flange yields. The beam flange yielding capacity,  $P_{bfy}$ :

$$P_{bfy} = F_y b_f t_f \quad (24)$$

where  $F_y$  is the beam flange yield stress.

The total thermal axial force,  $P_i$ , is the result of equal contribution of the top and bottom beam flanges. Thus, half the total thermal axial forces,  $P_i/2$ , and the external applied loads, acting in compression, are contributing to the applied force on the top beam flange,  $P_{af}$ :

$$P_{af} = \frac{P_i}{2} + \frac{M_{app}}{h_b - t_f} \quad (25)$$

When  $P_{af}$  reaches  $P_{bf}$ , yielding occurs in the top beam flange. Note that the bottom beam flange is still in the elastic state and  $\Delta P_{i(\text{compression})}$  can be calculated as a result of the bottom beam flange area (in elastic state) and the top beam flange area (in plastic state) contributions:

$$\Delta P_{i(\text{compression})} = \frac{KE_b b_f t_f \alpha \Delta T}{\left(\frac{E_b b_f t_f}{L} + K\right)} + \frac{KE_T b_f t_f \alpha \Delta T}{\left(\frac{E_T b_f t_f}{L} + K\right)} \quad (26)$$

where  $E_T$  is the tangent modulus of elasticity.

A ratio of  $(1/q_i)$  is multiplied by the elastic modulus of elasticity  $E$  to determine the tangent modulus of elasticity  $E_T$ . Note that  $q_i$  is the ratio of the plastic strain to the elastic strain at each temperature increment,  $\Delta T_i$ , which is obtained from the FE results of the parametric study presented in this paper. It is observed from the FE results that the beam plastification occurs at  $470^\circ C$  and  $q_i$  can be written as follows:

$$q_i = 50\sqrt{30/(500-T)} \quad \text{for } T \leq 470^\circ C \quad (27)$$

$$q_i = 50 \quad \text{for } T > 470^\circ C \quad (28)$$

d. Stage 3: top beam flange local buckling

Local buckling occurs after yielding of the top beam flange. The critical beam flange local buckling force,  $P_{crb}$  :

$$P_{crb} = \sigma_{avg} b_f t_f \quad (29)$$

where  $\sigma_{avg}$  is the average buckling stress found in [23].

Local flange buckling occurs when  $P_{atf}$  reaches  $P_{crb}$ . Only half the top beam flange area is assumed to be effective and contribute to the compressive axial force as per [24]. Note that the bottom beam flange is still in the elastic state and the incremental compressive axial force can be written as follows:

$$\Delta P_{i(\text{compression})} = \frac{KE_b b_f t_f \alpha \Delta T}{\left(\frac{E_b b_f t_f}{L} + K\right)} + \frac{0.5KE_T b_f t_f \alpha \Delta T}{\left(\frac{0.5E_T b_f t_f}{L} + K\right)} \quad (30)$$

e. Stage 4: bottom beam flange local buckling

Local buckling of the bottom beam flange occurs after the top beam flange buckles. And the applied force on bottom beam flange,  $P_{abf}$ , can be written as a function of the thermal induced axial forces acting in compression and the external applied loads acting in tension:

$$P_{abf} = \frac{P_i}{2} - \frac{M_{app}}{h_b - t_f} \quad (31)$$

Local buckling of the bottom beam flange occurs when  $P_{abf}$  reaches  $P_{crb}$ . Also, it is assumed that half the bottom beam flange area is effective and contribute to the compressive axial force as per [24]. And the incremental compressive axial force can be calculated as follows:

$$\Delta P_{i(\text{compression})} = \frac{0.5KE_b b_f t_f \alpha \Delta T}{\left(\frac{0.5E_b b_f t_f}{L} + K\right)} + \frac{0.5KE_T b_f t_f \alpha \Delta T}{\left(\frac{0.5E_T b_f t_f}{L} + K\right)} \quad (32)$$

f. Stage 5: bottom beam flange yielding

The onset of yielding of the bottom beam flange occurs right after the onset of buckling (when  $P_{abf}$  reaches  $P_{bfy}$ ). The incremental compressive axial force can be written as a function of an equivalent of one beam flange area (half the top beam flange area and half the bottom beam flange area):

$$\Delta P_{i(\text{compression})} = \frac{KE_T b_f t_f \alpha \Delta T}{\left(\frac{E_T b_f t_f}{L} + K\right)} \quad (33)$$

g. Stage 6: column flange and web yielding

The column flange yielding capacity,  $P_{cfy}$ , can be written as a function of the column flange effective length,  $l_{eff-cw}$ , and column flange thickness,  $t_{cf}$ :

$$P_{cfy} = F_{yc} l_{eff-cf} t_{cf} \quad (34)$$

where  $F_{yc}$  is the column yield stress.

The applied force on column flange,  $P_{acf}$ , can be written as a function of the thermal induced axial forces the external applied loads:

$$P_{acf} = \frac{P_i}{2} + \frac{M_f}{h_b + 2g} \quad (35)$$

where  $M_f$  is the moment applied at the face of the column ( $M_f = M_{pr} + V_h S_h$ , where  $M_{pr}$  is the maximum expected moment at plastic hinge in beam,  $V_h$  is the shear force at the plastic hinge in beam, and  $S_h$  is the location of the plastic hinge [19]). When  $P_{acf}$  reaches  $P_{cfy}$ , yielding of the column flange occurs.

The column web yielding capacity,  $P_{cwy}$ , can be written as a function of the column web effective depth,  $d_{cw}$ , and column web thickness,  $t_{cw}$ :

$$P_{cfy} = F_{yc} d_{cw} t_{cw} \quad (36)$$

The applied force on column web,  $P_{acw}$  is written as:

$$P_{acw} = \frac{P_i}{2} + \frac{M_f}{b_{eff-cw}} \quad (37)$$

When  $P_{acw}$  reaches  $P_{cwy}$ , column web yielding occurs.

After the onset of yielding, beam starts to sag and thermal tensile axial forces start to develop. These thermal tensile axial forces act as unloading forces on the beam and connection [2]. Thus,  $E_t$  is replaced by  $E_b$  and the incremental thermal tensile axial force at every temperature increment,  $\Delta T_i$ , is:

$$\Delta P_{i(tension)} = \frac{KE_b b_f t_f \alpha \Delta T}{\left(\frac{E_b b_f t_f}{L} + K\right)} \quad (38)$$

The total compressive axial force developed at every step  $i$  is calculated as follows:

$$P_i = P_{\max(compression)} - \Delta P_{i(tension)} \quad (39)$$

where  $P_{\max(compression)}$  is the maximum compressive axial force computed as the cumulative of all

$$\Delta P_{i(compression)}.$$

#### h. Stage 7: bottom shear bolts failure

Bottom shear bolts failure occurs at the onset of column flange and web yielding. Shear bolts capacity,  $P_{sb}$ , is a function of shear bolt ultimate strength,  $F_{ub}$ , and shear bolt area,  $A_{bolt}$ :

$$P_{sb} = 0.6 F_{ub} A_{bolt} \quad (40)$$

The applied force on bottom shear bolts,  $P_{abb}$ , can be written as a function of the thermal induced axial tensile forces and external applied loads:

$$P_{abb} = \frac{P_i - P_{\max(\text{compression})}}{2} + \frac{M_f}{h_b} \quad (41)$$

Note that bottom shear bolts failure occurs when  $P_{abb}$  reaches  $P_{sb}$ .

At the bottom shear bolt failure, the beam bottom flange has no contribution to the thermal tensile axial forces, and  $\Delta P_{i(\text{tension})}$  can be written as function of half the beam top flange area:

$$\Delta P_{i(\text{tension})} = \frac{0.5KE_b b_f t_f \alpha \Delta T}{\left(\frac{0.5E_b b_f t_f}{L} + K\right)} \quad (42)$$

i. Stage 8: beam-column contact

Contact between beam bottom flange and web, and column flange occurs when the connection rotation,  $\theta$ , reaches the geometric angle between column flange and beam bottom flange,  $\theta_{geom}$ :

$$\theta_{geom} = \tan^{-1}\left(\frac{SB}{h_b}\right) \quad (43)$$

where  $SB$  is the gap distance between the column and beam as shown in Fig. 7(b).

When contact occurs, beam web contributes to the thermal tensile axial forces and

$\Delta P_{i(\text{tension})}$  can be calculated as follows:

$$\Delta P_{i(\text{tension})} = \frac{KE_b (0.5b_f t_f + A_{bw}) \alpha \Delta T}{\left(\frac{E_b (0.5b_f t_f + A_{bw})}{L} + K\right)} \quad (44)$$

where  $A_{bw}$  is the area of the beam web ( $A_{bw} = t_{bw} (h_b - 2t_{bf})$ ), and  $t_{bw}$  is the thickness of the beam web).

j. Final stage: top shear bolts failure

For all cases presented in this paper, failure of top shear bolts occurs after the occurrence of the beam-column contact.

The applied force on top shear bolts,  $P_{atb}$  can be written as a function of the thermal induced tensile axial forces and the external applied loads:

$$P_{atb} = \frac{P_i - P_{\max(\text{compression})}}{2} - \frac{M_f}{h_b} \quad (45)$$

## 2. Effect of web angles

The proposed model is modified to include the effect of the web angles, the modification includes part of beam web area connected to web angles as shown in Fig. 15. The beam area included in the proposed model becomes:  $A_{bwa} = A_b + w_{wa} t_w$  (where  $w_{wa}$  is the web angles width).

Also, another modification is introduced to account for beam web yielding observed from FE results. This modification is introduced right after stage 4 (section 1.e). And the capacity,  $P_{bwy}$ , where beam web yielding occurs, can be written as a function of web angles width,  $w_{wa}$ , and beam web thickness,  $t_w$ :

$$P_{bwy} = F_y w_{wa} t_w \quad (46)$$

The applied force on beam web,  $P_{abw}$  can be calculated by multiplying the thermal induced compressive axial forces,  $P_i$ , by the ratio of the beam web area to the total area contributing to  $\Delta P_{i(\text{compression})}$ :

$$P_{abw} = P_i \left( \frac{w_{wa} t_w}{w_{wa} t_w + 2b_f t_f} \right) \quad (47)$$

Yielding of the beam web area in contact with web angles occurs when  $P_{abw}$  reaches  $P_{bwy}$ , and the incremental compressive axial forces,  $\Delta P_{i(\text{compression})}$ , can be written as follows:

$$\Delta P_{i(\text{compression})} = \frac{KE_b(0.5b_f t_f)\alpha\Delta T}{\left(\frac{E_b(0.5b_f t_f)}{L} + K\right)} + \frac{KE_T(0.5b_f t_f + w_{wa} t_w)\alpha\Delta T}{\left(\frac{E_T(0.5b_f t_f + w_{wa} t_w)}{L} + K\right)} \quad (48)$$

After modifying the area of beam by including the contribution of the beam web area ( $A_b$  is replaced by  $A_{bwa}$ ), Equations 19 to 45 can be used in predicting the thermal induced axial forces,  $P_i$ , at each limit state till shear bolt failure occurs.

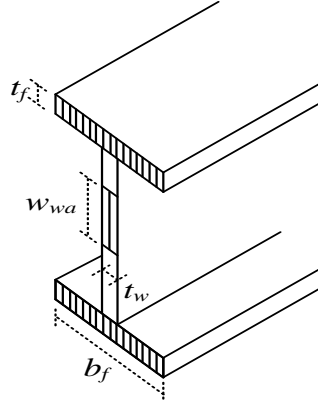


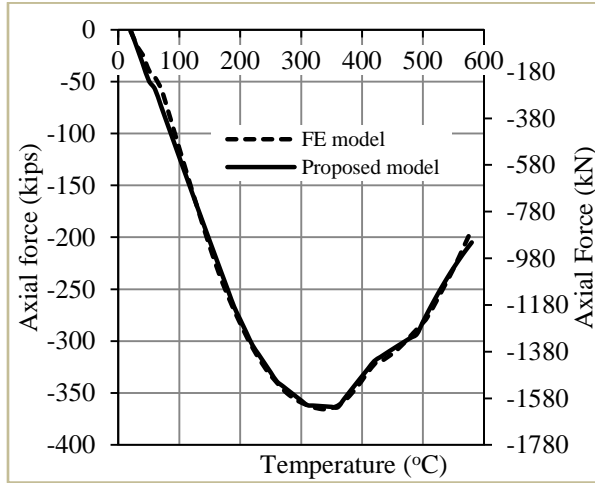
**Figure. 15.** Beam area  $A_{bwa}$ .

### 3. Proposed model performance

A comparison of the proposed model with FE results of typical cases of the parametric study is presented. Figures 9 and 10 show the axial force-temperature and temperature-rotation responses of the connection with and without web angles, respectively. It can be seen that the proposed model predicts the axial force and the rotation with excellent agreement when compared with FE results for all presented cases. The model predicts all possible limit states, failure modes, and failure temperatures.



(a)



(b)

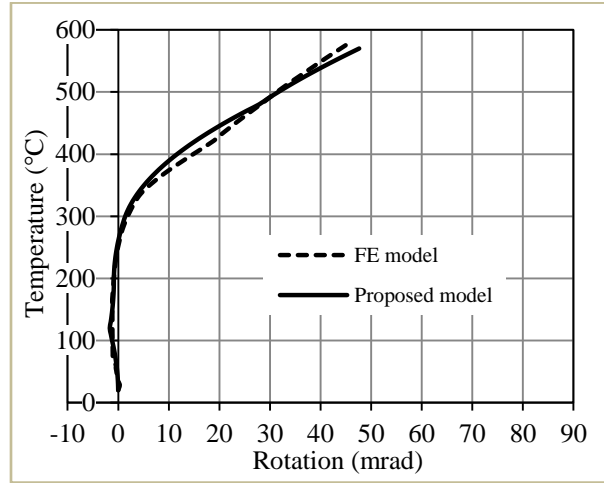
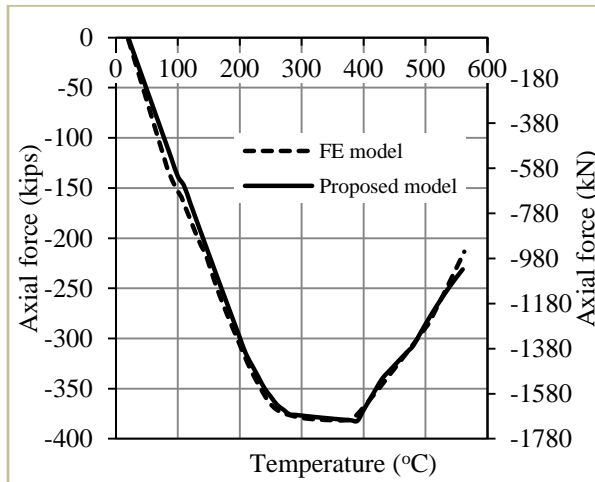


**Figure 16.** FE vs. proposed model for case 1: (a) Axial Force, (b) Connection rotation.

(a)



(b)

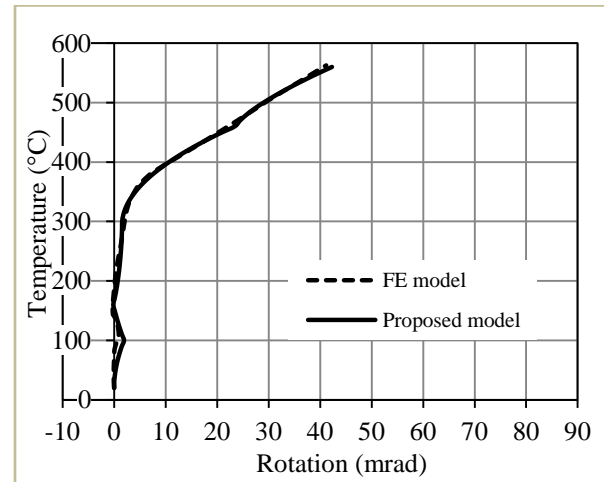
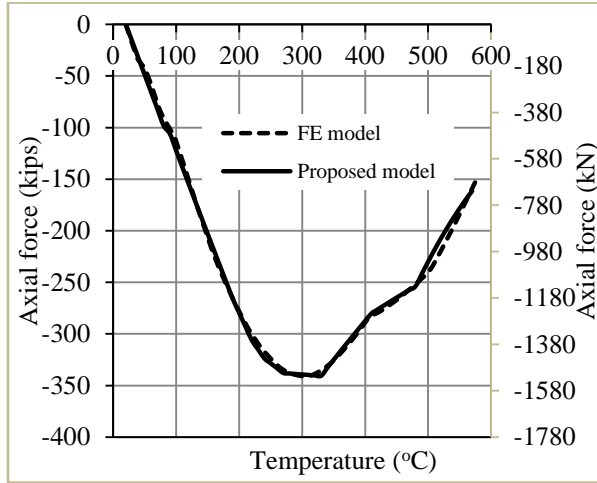


**Figure 17.** FE vs. proposed model for case 2: (a) Axial Force, (b) Connection rotation.

(a)



(b)

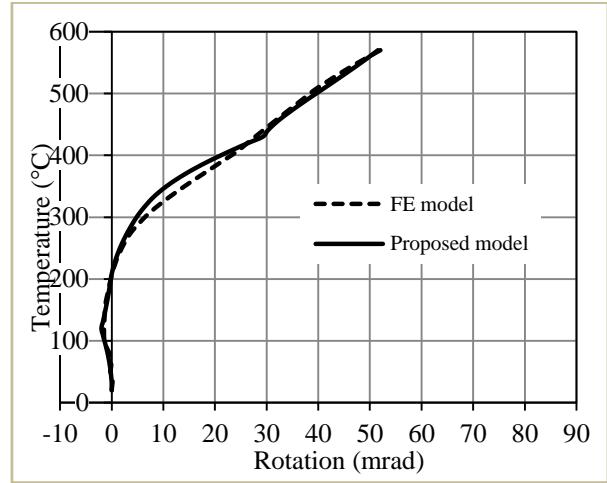
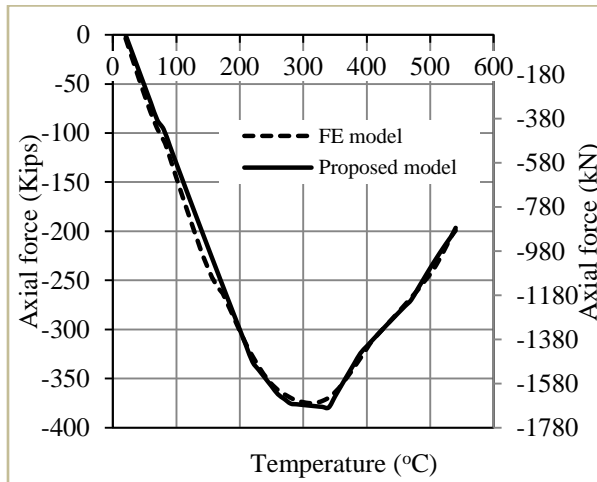


**Figure 18.** FE vs. proposed model for case 3: (a) Axial Force, (b) Connection rotation.

(a)



(b)

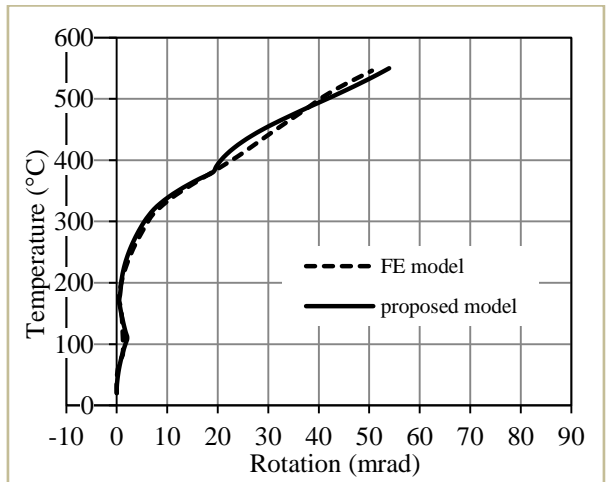
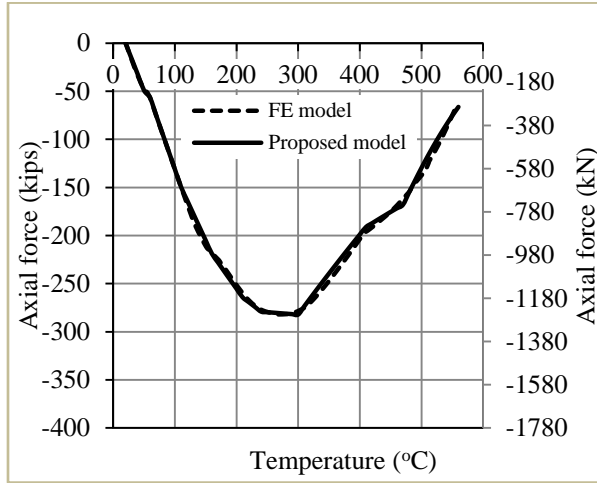


**Figure 19.** FE vs. proposed model for case 4: (a) Axial Force, (b) Connection rotation.

(a)



(b)

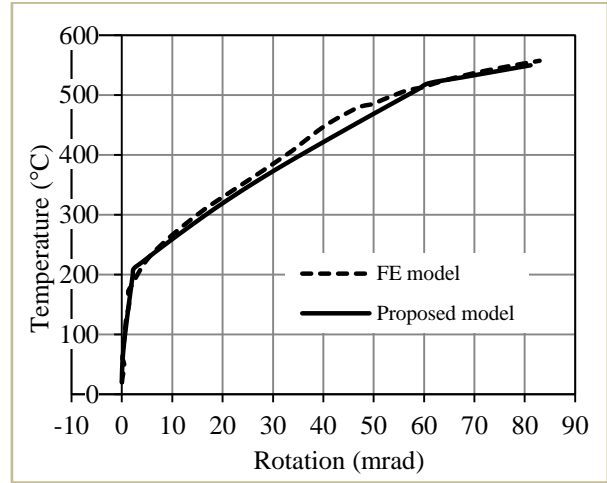
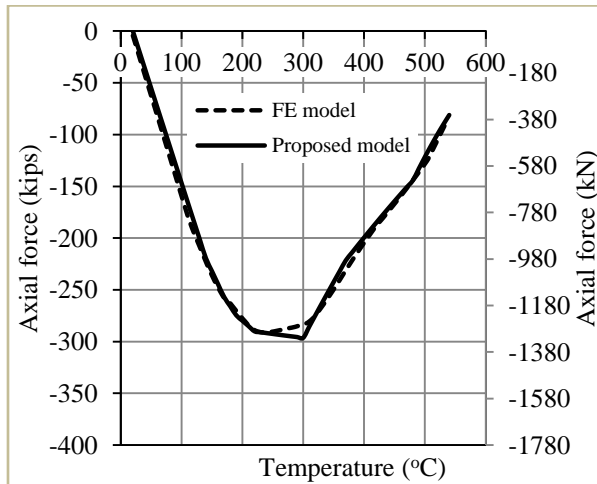


**Figure 20.** FE vs. proposed model for case 5: (a) Axial Force, (b) Connection rotation.

(a)



(b)

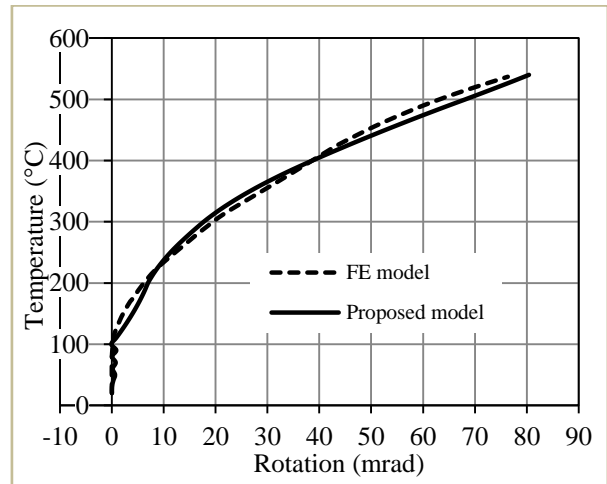
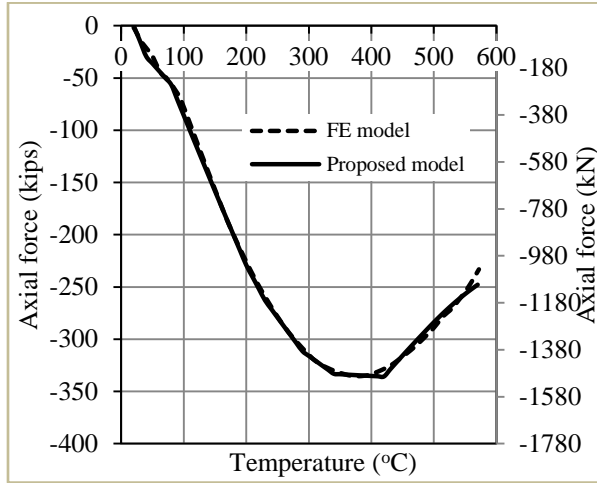


**Figure 21.** FE vs. proposed model for case 6: (a) Axial Force, (b) Connection rotation.

(a)



(b)

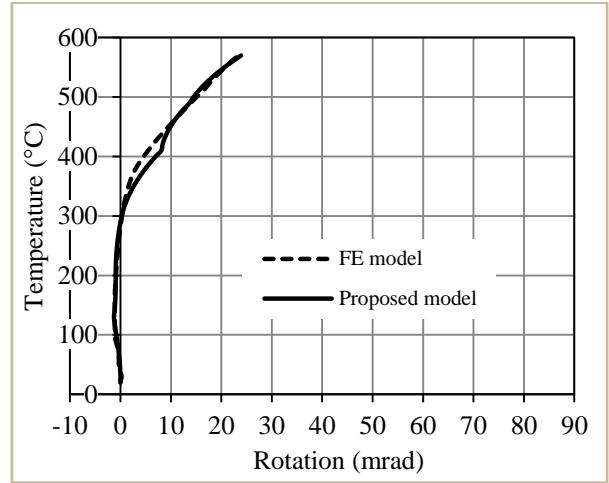
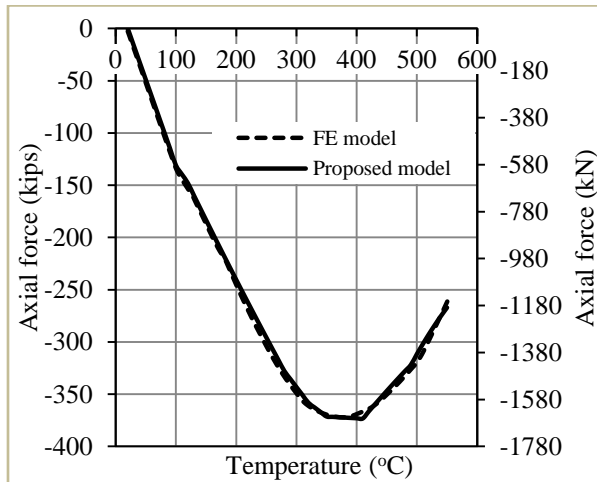


**Figure. 22.** FE vs. proposed model for case 7: (a) Axial Force, (b) Connection rotation.

(a)



(b)

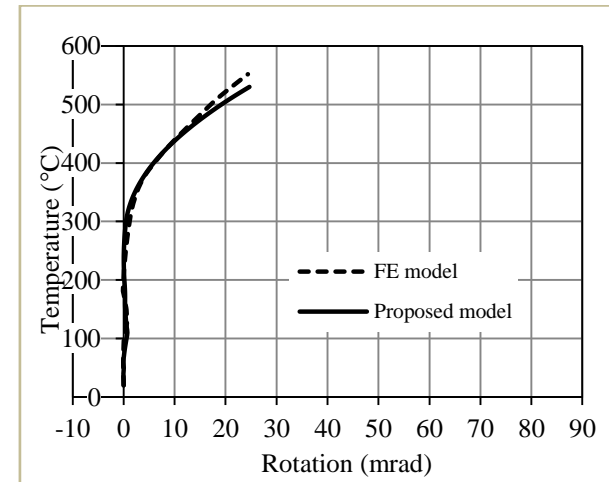
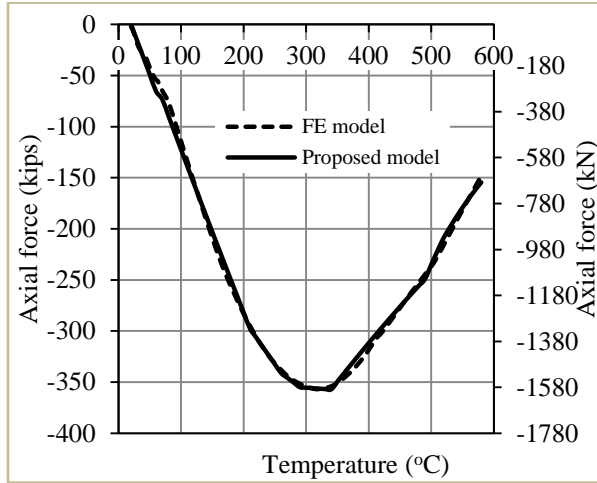


**Figure. 23.** FE vs. proposed model for case 8: (a) Axial Force, (b) Connection rotation.

(a)



(b)

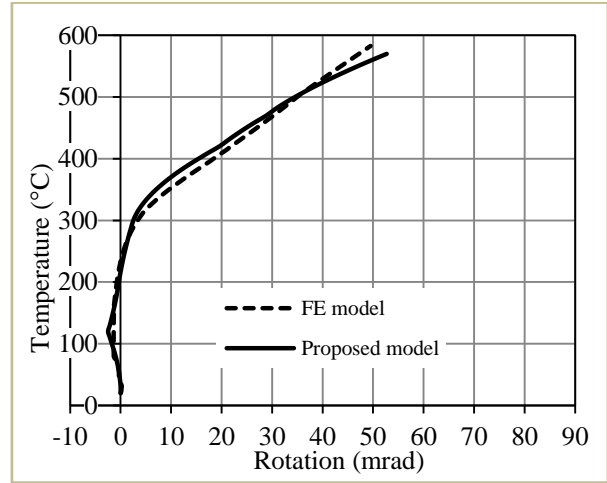
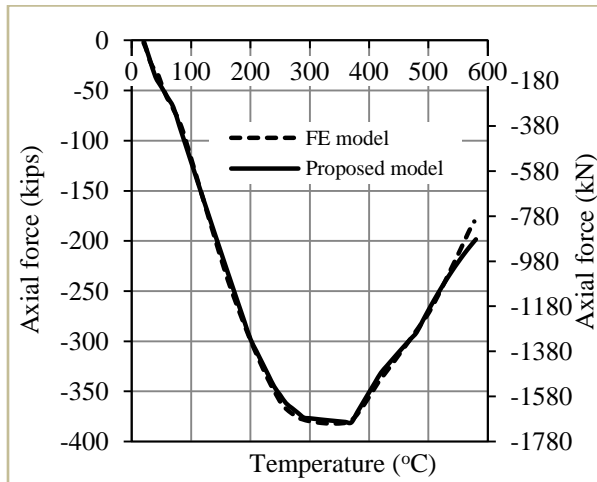


**Figure. 24.** FE vs. proposed model for case 9: (a) Axial Force, (b) Connection rotation.

(a)



(b)

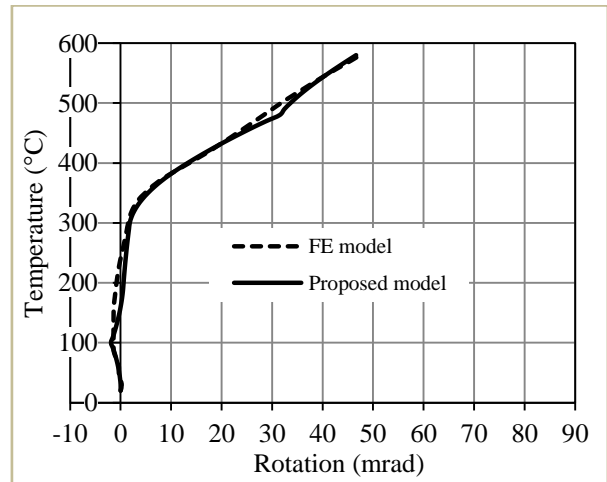
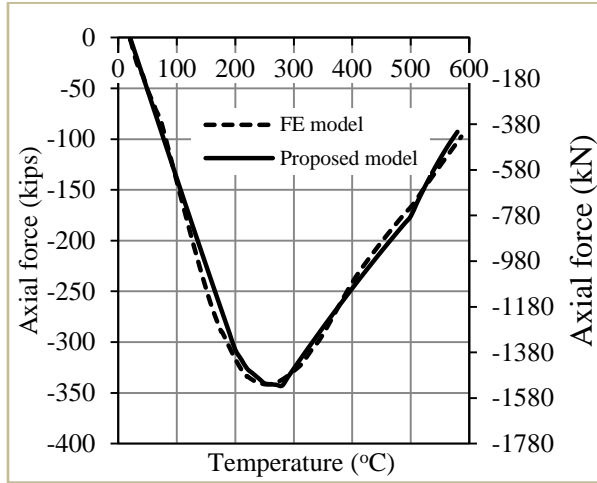


**Figure. 25.** FE vs. proposed model for case 10: (a) Axial Force, (b) Connection rotation.

(a)



(b)

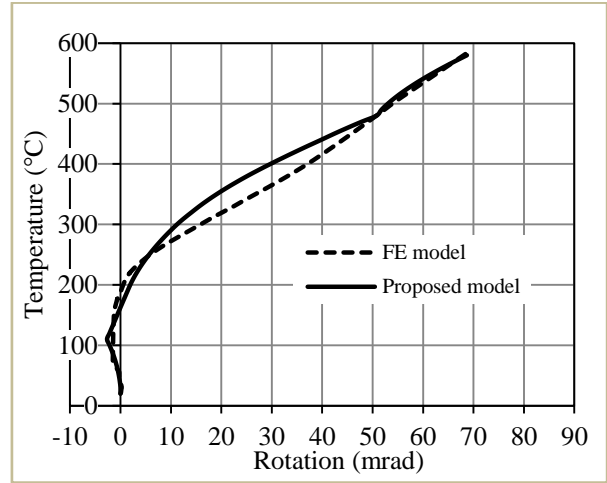
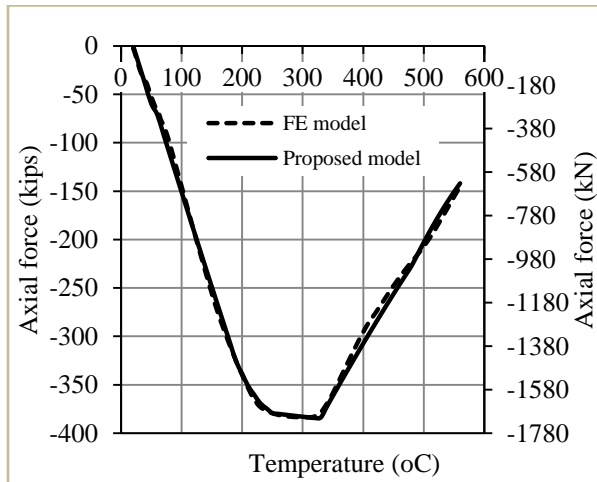


**Figure. 26.** FE vs. proposed model for case 11: (a) Axial Force, (b) Connection rotation.

(a)



(b)

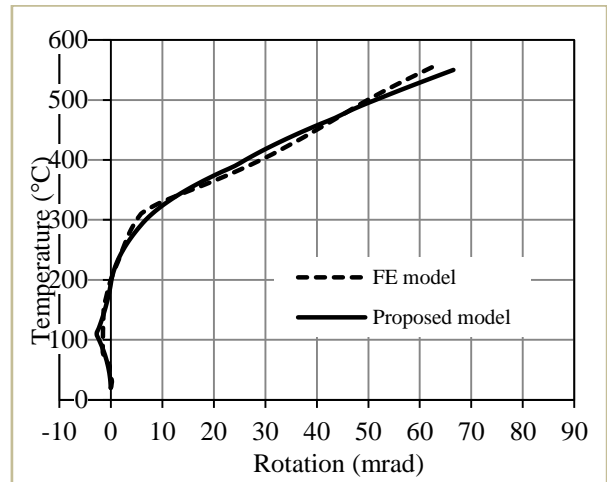
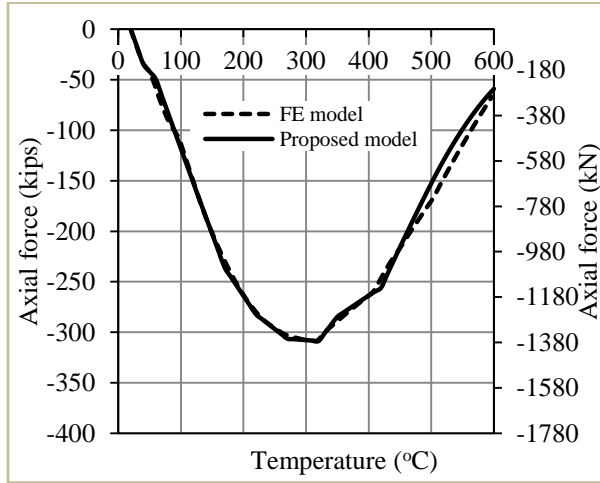


**Figure. 27.** FE vs. proposed model for case 12: (a) Axial Force, (b) Connection rotation.

(a)



(b)

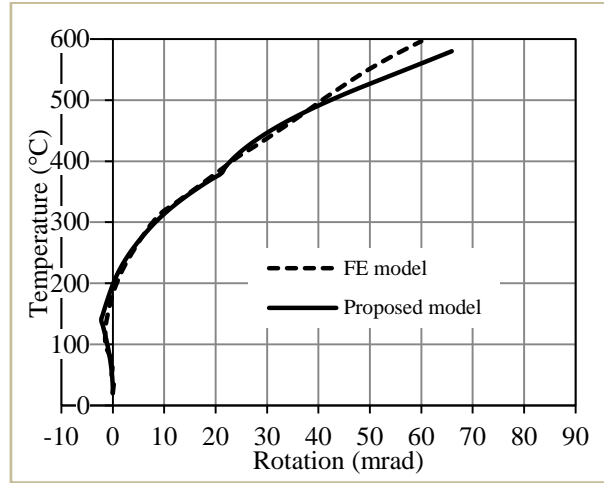
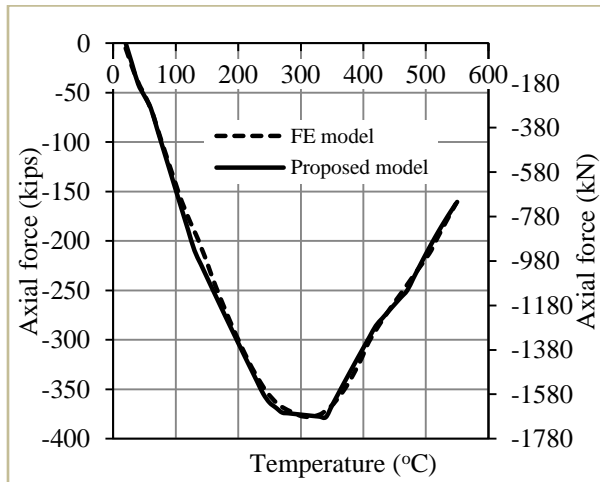


**Figure. 28.** FE vs. proposed model for case 13: (a) Axial Force, (b) Connection rotation.

(a)



(b)

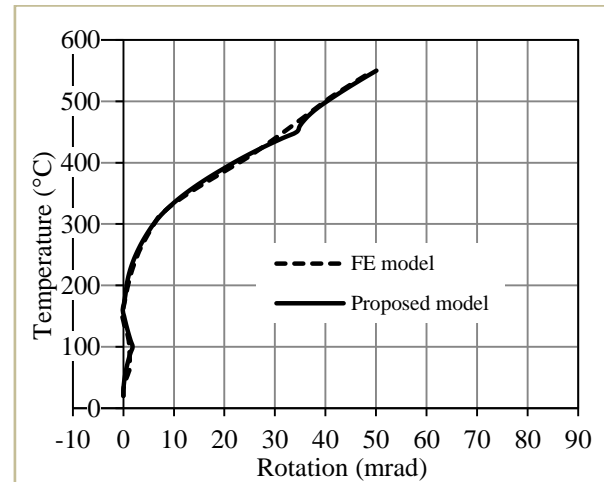
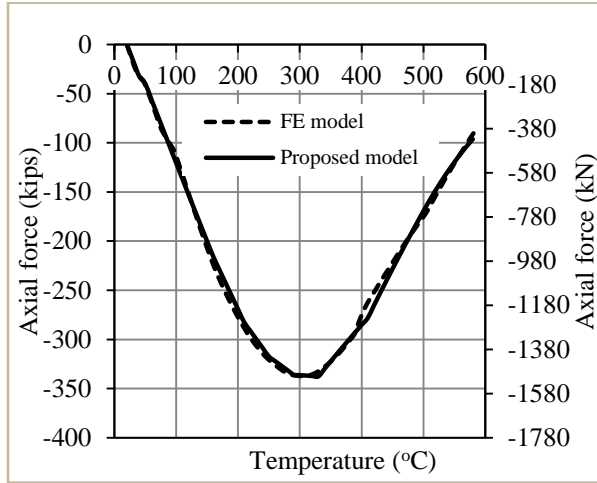


**Figure. 29.** FE vs. proposed model for case 14: (a) Axial Force, (b) Connection rotation.

(a)



(b)

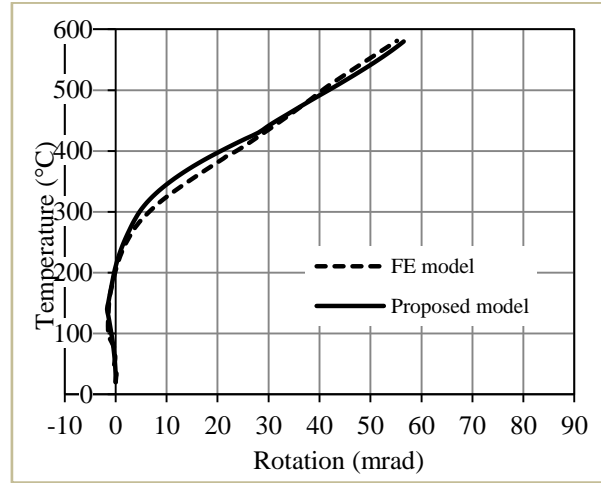
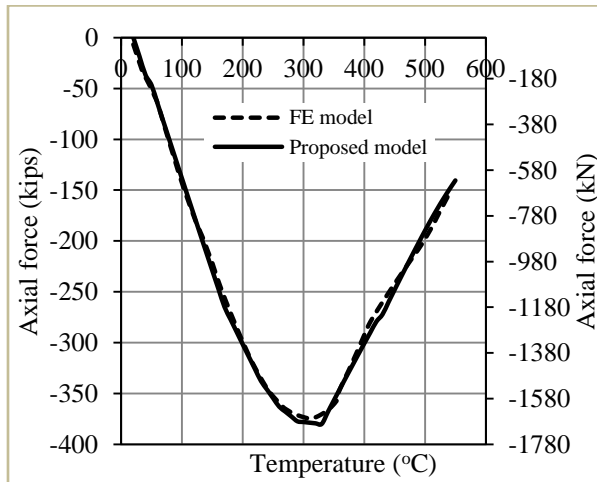


**Figure. 30.** FE vs. proposed model for case 15: (a) Axial Force, (b) Connection rotation.

(a)



(b)

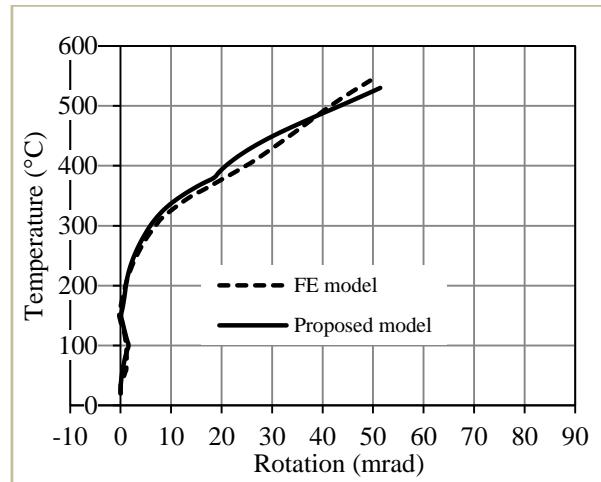


**Figure. 31.** FE vs. proposed model for case 16: (a) Axial Force, (b) Connection rotation.

Table 4 shows a comparison between the proposed model and FE results. The temperature at failure, maximum compressive axial force, and maximum rotation are presented in Table 4 for both mechanical model and FE results. The percentage differences between the mechanical model and the FE results are shown to be acceptable. Note that shear bolt failure is the governing failure mode for all cases.



**Table 4.** FE vs. proposed model results of top and seat angle connection assembly.

Case	Model	Failure mode	Temperature at failure (°C)		Maximum compressive axial force (kips)		Maximum rotation (mrad)	
			Temperature (°C)	% difference (model vs. FE)	Axial force (kips)	% difference (model vs. FE)	Rotation (mrad)	% difference (model vs. FE)
1	FE	Top and seat shear bolts	576	-	366.00	-	45.00	-
1	Mechanical		570	-1.04%	364.00	-0.55%	48.00	6.67%
2	FE		562	-	382.00	-	41.00	-
2	Mechanical		560	-0.36%	386.00	1.05%	42.00	2.44%
3	FE		574	-	341.00	-	53.00	-
3	Mechanical		570	-0.70%	338.00	-0.88%	52.00	-1.89%
4	FE		546	-	375.00	-	51.00	-
4	Mechanical		540	-1.10%	382.00	1.87%	54.00	5.88%
5	FE		557	-	282.00	-	83.00	-
5	Mechanical		560	0.54%	283.00	0.35%	81.00	-2.41%
6	FE		537	-	282.00	-	76.00	-
6	Mechanical		530	-1.30%	283.00	0.35%	80.00	5.26%
7	FE		572	-	336.00	-	24.00	-
7	Mechanical		570	-0.35%	332.00	-1.19%	24.00	0.00%
8	FE		552	-	372.00	-	24.00	-
8	Mechanical		550	-0.36%	332.00	-10.75%	27.00	12.50%
9	FE		583	-	357.00	-	49.00	-
9	Mechanical		580	-0.51%	361.00	1.12%	53.00	8.16%
10	FE		577	-	382.00	-	47.00	-
10	Mechanical		580	0.52%	388.00	1.57%	47.00	0.00%
11	FE		586	-	342.00	-	69.00	-
11	Mechanical		580	-1.02%	342.00	0.00%	69.00	0.00%
12	FE		556	-	384.00	-	63.00	-
12	Mechanical		560	0.72%	387.00	0.78%	67.00	6.35%
13	FE		596	-	309.00	-	60.00	-
13	Mechanical		600	0.67%	311.00	0.65%	66.00	10.00%
14	FE		547	-	378.00	-	49.00	-
14	Mechanical		550	0.55%	377.00	-0.26%	50.00	2.04%
15	FE		581	-	338.00	-	55.00	-
15	Mechanical		580	-0.17%	336.00	-0.60%	57.00	3.64%
16	FE		542	-	375.00	-	49.00	-
16	Mechanical		540	-0.37%	375.00	0.00%	54.00	10.20%

Two additional top and seat angle connections, were designed using W18x46 and W21x68 beam section for validation purposes. The designed models were developed in ABAQUS and validated against the proposed model. Results of axial force-temperature and

temperature-rotation of the FE and mechanical models show that the proposed model is able to predict, with acceptable agreement, the behavior of top and seat angle connections under varied geometric and loading conditions (see Figs. 31 and 32).

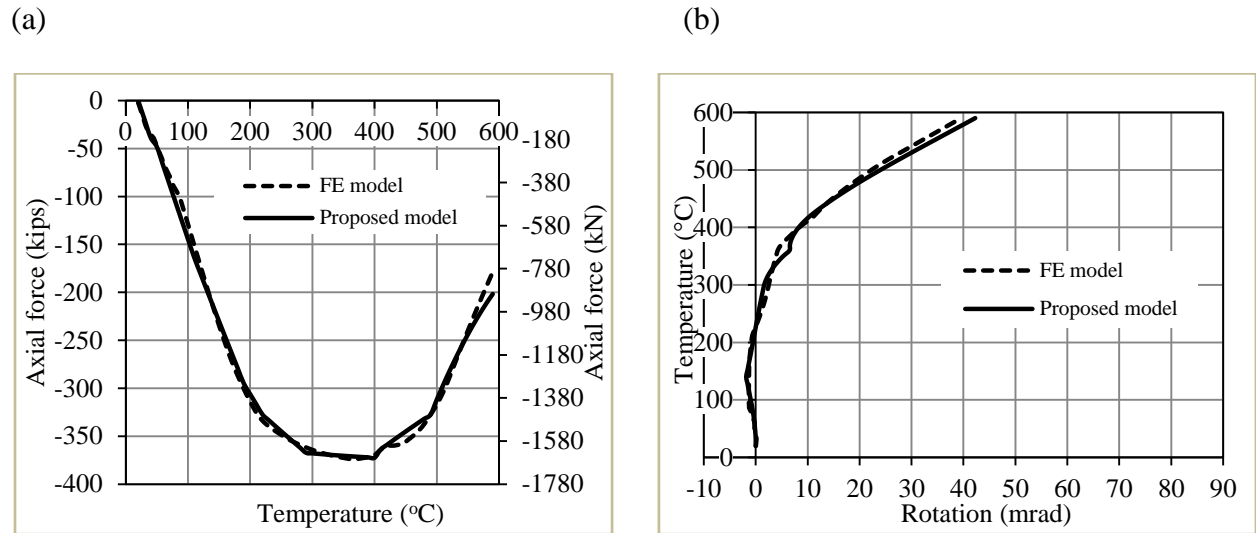


**Figure. 32.** FE vs. proposed model for W18x46 beam: (a) Axial Force, (b) Connection rotation.

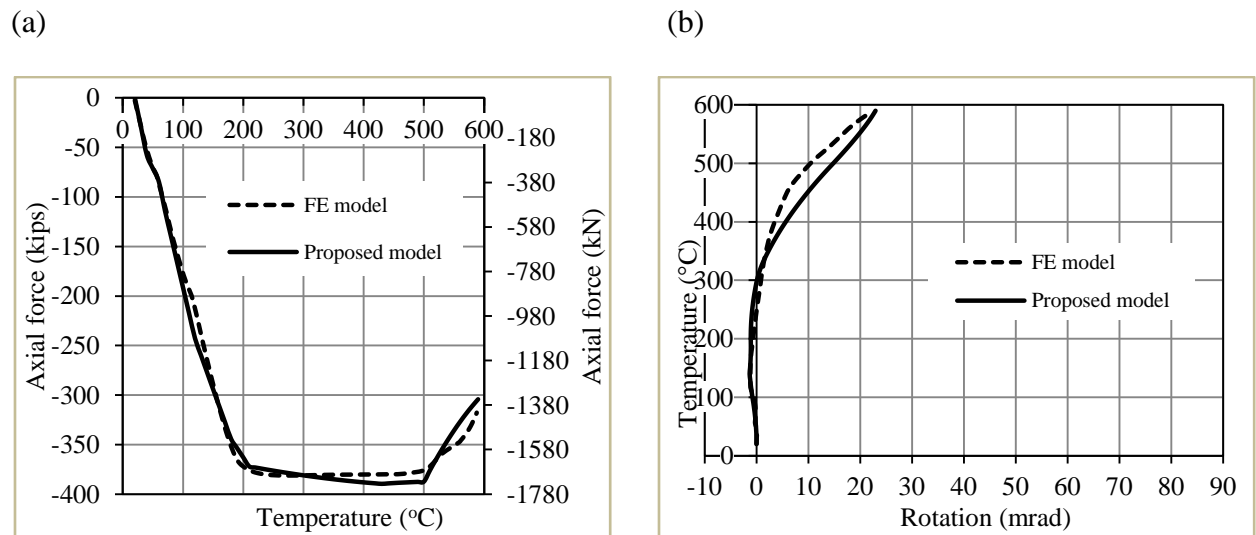


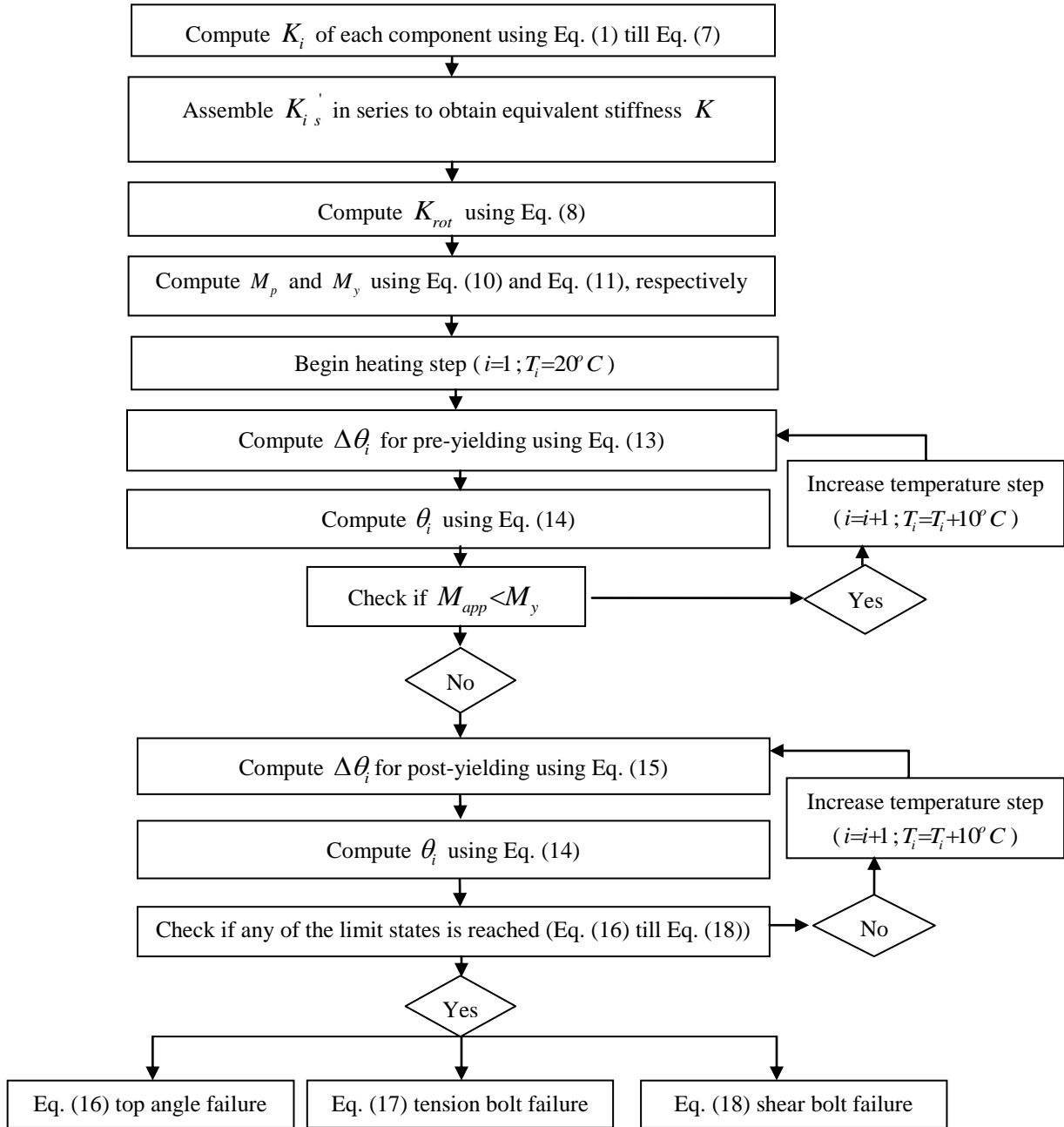
**Figure. 33.** FE vs. proposed model for W21x68 beam: (a) Axial Force, (b) Connection rotation.

### **E. Automated procedure**

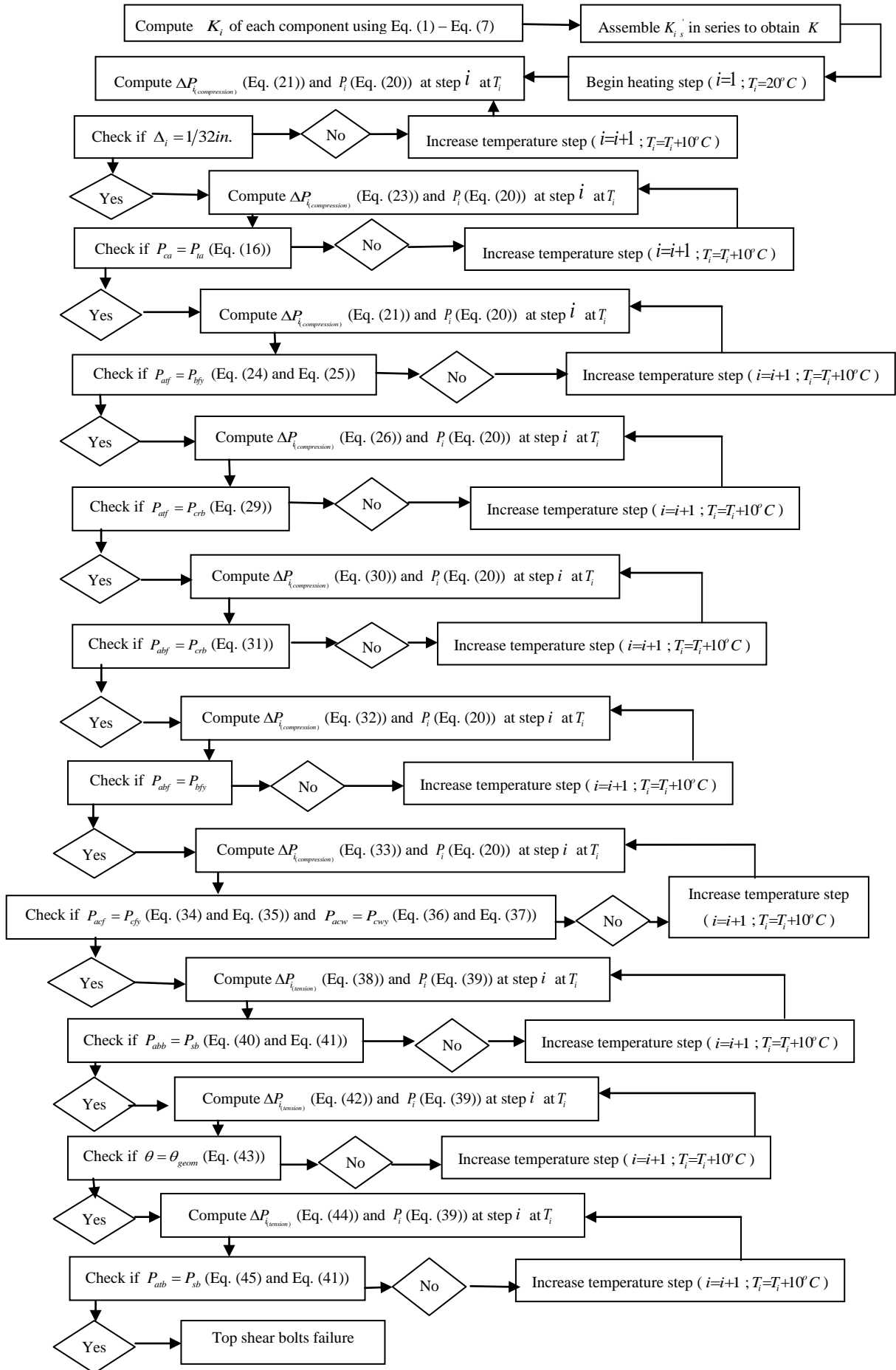
The mechanical model is developed to be applied in an incremental computer automated iterative solution as shown in Fig. 34. An engineer would start by determining the stiffness of the different components of the connection. Next, the equivalent stiffness,  $K$ , is computed. The engineer refers to Fig. 34(a) to predict the temperature-rotation response, and Fig. 34(b) to predict the axial force-temperature response of top and seat angle connections. At each temperature increment, the total, rotation and thermal axial force are calculated. The process is repeated again until the following limit state is reached. At each limit state, corresponding equations of incremental rotation and thermal axial force are used, and the process is repeated until connection failure occurs.

**Figure. 34.** Flowchart of the incremental mechanical model: (a) rotation, (b) axial force.

(a)



(b)



## CHAPTER V

### SUMMARY, CONCLUSIONS AND RECOMMENDATIONS

#### **A. Summary and conclusions**

A mechanical model that predicts the thermal induced axial forces, connection rotation, and failure was developed for top and seat angle connections with and without web angles subjected to fire loading.

For this purpose, FE models of the connection were developed and validated against experimental results available in the literature [6]. Also, FE models for the beam-column connection assembly were used to conduct a parametric study to investigate the effect of key geometric parameters on the behavior of such connections during a fire event. Results of the parametric study showed that these connections are vulnerable to failure during the heating stage of a fire at temperatures ranging between 530°C and 600°C. The governing failure mode was shear bolt failure.

The results of all FE models and existing experimental results available in literature [6] were used to develop a mechanical model that allows engineers to quantify the temperature-rotation and axial force-temperature response of top and seat angle connections with and without web angles. The proposed model showed that adding the effect of the beam component changes the response and failure mode of top and seat angle connections. The results of the proposed model showed excellent agreement when compared with experimental and FE results.

An automated iterative solution was proposed to allow design engineers to quantify thermal induced axial forces on top and seat angle connections and incorporate them into the design of such connections. One of the main advantages of the proposed mechanical model is

that, in addition to its accuracy, it requires much less computational effort than that required using FE analysis, and can be used as well in more advanced modeling applications for fire analysis and design.

It is important to note that the proposed model has two limitations. One is that prying effect on top and seat angles were not included in the formulation. Another limitation is that the model is applicable only for slender beam flanges as defined in Selamet and Garlock [23].

## **B. Recommendations**

More research work is still needed in order to develop a full understanding of the connection response to fire.

- Prying forces effect on tension bolts are needed to be incorporated in the formulation of the proposed mechanical model.
- A fracture model is needed to be adopted in all FE models which allows a post-yielding analysis of the connection response to fire.
- The effect of different fire scenarios on the connection response is needed to be investigated and the creep effect on bolts and base material is need to be investigated as well.
- Additional experimental work on full scale tests, including the beam effect, is needed to be conducted for validation purposes.

## BIBLIOGRAPHY

- [1] Agarwal, A., Selden, K., Varma, A., Stability behavior of steel building structures in fire conditions: Role of composite floor system with shear-tab connections, Journal of Structural Fire Engineering, 2014, 5(2), 77-96.
- [2] Taib, M., Burgess, I.W., A component-based model for fin-plate connections in fire, Journal of Structural Fire Engineering, 2013, 4(2), 113-122.
- [3] Eurocode 3- Design of steel structures- part 1.8: Design of Joints, EN 1995-1-8 CEN, European Committee for Standardization, Brussels, Belgium.
- [4] Salajegheh, E., Gholizadeh, S., Pirmoz, A., Self-organizing back propagation networks for predicting the moment-rotation behavior of bolted connections, Asian Journal of Civil Engineering, 2008, 9(6), 629-645.
- [5] Pirmoz, A., Khoei, A.S., Mohammadzerapour, E., Saedi D., A., Moment-rotation behavior of bolted top-seat angle connections, Journal of Constructional Steel Research, 2009, 65(4), 973-984.
- [6] Saedi D., A., Yahyai, M., Behavior of bolted top-seat angle connections in fire, Journal of Constructional Steel Research, 2009, 65(3), 531-541.
- [7] Yuan, Z., Tan, K.H., Ting, S.K., Testing of composite steel top-and-seat-and-web angle joints at ambient and elevated temperatures: Part 2—Elevated-temperature tests, Engineering Structures, 2011, 33(7), 2093-2109.
- [8] Saedi D., A., Yahyai, M., Modeling of bolted angle connections in fire, Fire Safety Journal, 2009, 44(7), 976-988.
- [9] Yahyai, M., Behzadpoori, M., Saedi D., A., Baleh, M.A., The simple model for bolted connections in fire, Engineering, 2011, 3(9), 865-875.



- [10] Reinoso, J.M., Loureiro, A., Gutierrez, R., Lopez, M., Analytical frame approach for the rotational stiffness prediction of beam-to-column angle connections, Journal of Constructional Steel Research, 2015, 106, 67-76.
- [11] Yang, J., Choi, J., Kim, S., A Finite element model for the prediction of the behavior of an unstiffened top and seat angle connection with various top angle bolt gage distances, Journal of Asian Architecture and Building Engineering, 2011, 10(2), 367-374.
- [12] Ellifritt, D.S., Sputo, T., Design criteria for stiffened seated connections to column webs, Engineering Journal, 1999, 36(4), 160-168.
- [13] Weynand, K., Jaspart, J.P. Steenhuis, M., The stiffness model of revised Annex J of Eurocode 3, Connections in steel structures III: Proceedings of the Third International Workshop on Connections in Steel Structures, Oxford, 1995, 441-452.
- [14] Pirmoz, A., Saedi D., A., Mazaheri, A. Darbandi, H.E., Behavior of bolted angle connections subjected to combined shear force and moment, Journal of Constructional Steel Research, 2008, 64(4), 436-446.
- [15] Pietrapertosa, C., Jaspart, J.P., Ductility requirements in shear bolted connections, Connections in Steel Structures V, Amsterdam, June 3-4, 2004, 335-345.
- [16] Yang, B., Tan, K., Component-based model of bolted-angle connections subjected to catenary action, Proceedings of the 10th International Conference on Advances in Steel Concrete Composite and Hybrid Structures, Singapore, 2012, 654-661.
- [17] AISC. Specification for structural steel buildings, Standard ANSI/AISC 360-10. Chicago, IL: American Institute of Steel Construction, Inc., 2010.
- [18] Eurocode 3- Design of steel structures - part 1.2: General rules structural fire design (drafts), EN 1995-1-2 CEN, European Committee for Standardization, Brussels, Belgium.

- [19] Schippers, J., Design procedure for bolted top-and-seat angle connections for use in seismic applications, M.S. thesis. University of Cincinnati, 2012.
- [20] Hu, G., Engelhardt, M., Studies on the behaviour of steel single-plate beam end connections in a fire, Structural Engineering International: Journal of the International Association for Bridge and Structural Engineering (IABSE), 2012, 22(4), 462-469.
- [21] Lee, J., Morovat, M.A., Hu, G., Engelhardt, M.D., Taleff, E.M., Experimental investigation of mechanical properties of ASTM A992 steel at elevated temperatures, Engineering Journal, 2013, 50(4), 249-272.
- [22] Johnston, R., Lim, J., Sonebi, M., Wrzesien, A., Armstrong, C., The structural behavior in fire of a cold-formed steel portal frame having semi-rigid joints, Journal of Structural Fire Engineering, 2015, 6(2), 77-101.
- [23] Selamet, S., Garlock, M., Plate buckling of steel wide-flange sections at elevated temperatures, Journal of Structural Engineering, 2013, 139(11), 1853-1865.
- [24] Rhodes, J., Some observations on the post-buckling behaviour of thin plates and thin-walled members, Thin-Walled Structures, 2003, 41(2-3), 207-226.

